ELSEVIER

Institut Pasteur

Microbes and Infection 15 (2013) 56–65

www.elsevier.com/locate/micinf

Original article

Gag-CA Q110D mutation elicits TRIM5-independent enhancement of HIV-1mt replication in macaque cells

Masako Nomaguchi [a,1], Masaru Yokoyama [b,1], Ken Kono [c], Emi E. Nakayama [c], Tatsuo Shioda [c], Akatsuki Saito [d], Hirofumi Akari [d], Yasuhiro Yasutomi [e], Tetsuro Matano [f], Hironori Sato [b], Akio Adachi [a,*]

[a] *Department of Microbiology, Institute of Health Biosciences, The University of Tokushima Graduate School, 3-18-15 Kuramoto, Tokushima 770-8503, Japan*
[b] *Laboratory of Viral Genomics, Pathogen Genomics Center, National Institute of Infectious Diseases, 4-7-1 Gakuen, Musashimurayama, Tokyo 208-0011, Japan*
[c] *Department of Viral Infections, Research Institute for Microbial Diseases, Osaka University, 3-1 Yamadaoka, Suita, Osaka 565-0871, Japan*
[d] *Center for Human Evolution Modeling Research, Primate Research Institute, Kyoto University, 41-2 Kanrin, Inuyama, Aichi 484-8506, Japan*
[e] *Tsukuba Primate Research Center, National Institute of Biomedical Innovation, Tsukuba, Ibaraki 305-0843, Japan*
[f] *AIDS Research Center, National Institute of Infectious Diseases, 1-23-1 Toyama, Shinjuku-ku, Tokyo 162-8640, Japan*

Received 5 September 2012; accepted 20 October 2012
Available online 1 November 2012

Abstract

HIV-1 is strictly adapted to humans, and cause disease-inducing persistent infection only in humans. We have generated a series of macaque-tropic HIV-1 (HIV-1mt) to establish non-human primate models for basic and clinical studies. HIV-1mt clones available to date grow poorly in macaque cells relative to SIVmac239. In this study, viral adaptive mutation in macaque cells, G114E in capsid (CA) helix 6 of HIV-1mt, that enhances viral replication was identified. Computer-assisted structural analysis predicted that another Q110D mutation in CA helix 6 would also increase viral growth potential. A new proviral construct MN4Rh-3 carrying CA-Q110D exhibited exquisitely enhanced growth property specifically in macaque cells. Susceptibility of MN4Rh-3 to macaque TRIM5α/TRIMCyp proteins was examined by their expression systems. HIV-1mt clones so far constructed already completely evaded TRIMCyp restriction, and further enhancement of TRIMCyp resistance by Q110D was not observed. In addition, Q110D did not contribute to evasion from TRIM5α restriction. However, the single-cycle infectivity of MN4Rh-3 in macaque cells was enhanced relative to the other HIV-1mt clones. Our results here indicate that CA-Q110D accelerates viral growth in macaque cells irrelevant to TRIM5 proteins restriction.

Keywords: HIV-1; HIV-1mt; Gag-CA; Macaque cells; Virus growth; Molecular modeling

1. Introduction

Mammalian cells express a variety of host restriction factors to defend themselves against pathogens. Viruses have evolved countermeasures to subvert their restriction and replicate efficiently in cells [1,2]. HIV-1, a causative agent of human AIDS, evades host restriction factors and replicates well in human cells. However, in macaques for experimental use, e.g. cynomolgus macaques (CyMs) and rhesus macaques (RhMs), HIV-1 replication is completely inhibited by host restriction factors present in their cells [3]. Construction of HIV-1 that overcomes species-barrier contributes much to understand the interaction of HIV-1 and its host as well as the establishment of HIV-1-infected macaque models [4,5].

Extensive molecular biological studies on the HIV-1/host interaction conducted to date have revealed main mechanical bases for the narrow host range exhibited by HIV-1. Macaque cells contain potent antiviral factors that effectively restrict or even abolish HIV-1 replication. These include APOBEC3 proteins (APOs), CyclophilinA (CypA), and TRIM5α/TRIMCyp

* Corresponding author. Tel.: +81 88 633 7078; fax: +81 88 633 7080.
E-mail address: adachi@basic.med.tokushima-u.ac.jp (A. Adachi).
[1] Masako Nomaguchi and Masaru Yokoyama contributed equally to this work.

1286-4579/$ - see front matter © 2012 Institut Pasteur. Published by Elsevier Masson SAS. All rights reserved.
http://dx.doi.org/10.1016/j.micinf.2012.10.013

(TRIM5 proteins). HIV-1 can indeed counteract human proteins corresponding to these restriction factors. APOs exhibit cytidine deaminase activity, and introduce lethal mutations into HIV-1 genome. HIV-1 Vif is able to neutralize the antiviral activity of human APOs, but not macaque APOs [6–8]. CypA acts on incoming HIV-1 core to regulate infection positively in human cells but negatively in macaque cells [9–11], though amino acid sequences of CypA from human and macaque are identical. Macaque TRIM5α recognizes and interacts with incoming HIV-1 core, and restricts virus infection in a less-defined mechanism [9–11]. Macaque TRIM5α is polymorphic, and has sequence variation in a C-terminal B30.2/SPRY domain important for capsid (CA) binding. Sequence variation in this domain causes modulation of host susceptibility to retrovirus infection [12,13]. Macaque TRIMCyp is a fusion protein resulted from replacement of a B30.2/SPRY domain with CypA. Both CyM and RhM cells express TRIMCyp, but affinity of these proteins to HIV-1 core is different due to amino acid substitutions in Cyp domains. Thus, CyM TRIMCyp restricts HIV-1 replication, but not RhM TRIMCyp [14,15].

Identification of host restriction factors in macaque cells and their target proteins in HIV-1 has prompted us to generate macaque-tropic HIV-1 (HIV-1mt) with a minimal modification of HIV-1 genome. We successfully constructed prototype HIV-1mt, NL-DT5R, by replacing CypA binding region on a loop between helices 4 and 5 (h4/5L) in *gag*-CA and entire *vif* genes with the corresponding regions of pathogenic SIVmac239 (Fig. 1) [16]. But growth potential of NL-DT5R was inferior to that of SIVmac239 both *in vitro* and *in vivo* [16,17]. These results indicated that genetic modifications in NL-DT5R were insufficient to confer the ability on the virus to grow efficiently in macaque cells [16–18]. In an attempt to improve growth potential of NL-DT5R, we adapted NL-DT5R and its R5-tropic version NL-DT562 to a CyM derived lymphocyte cell line HSC-F, and found a number of genetic substitutions in viral genomes of adapted viruses [19]. We introduced these mutations and CA h6/7L from SIVmac239 into NL-DT5R, and the resultant clone was designated MN4-5S (Fig. 1) [19]. MN4-5S exhibited enhanced growth potential in CyM both *in vitro* and *in vivo* compared to NL-DT5R [19]. But growth ability of MN4-5S was still lower than that of SIVmac239.

In this study, to further improve replication potential of HIV-1mt, we adapted MN4-5S in macaque cells and identified an adaptive mutation in CA that enhances growth ability in the cells. *In silico* structural modeling of the adaptive mutation predicted that Q110D mutation on helix 6 in CA (CA-Q110D) would promote viral replication in macaque cells. Indeed, a proviral clone carrying CA-Q110D, designated MN4Rh-3, exhibited marked enhancement of growth potential in macaque cells relative to all the other HIV-1mt clones we have constructed (Fig. 1). CyM TRIM5α/TRIMCyp susceptibility assays revealed that MN4Rh-3 completely evades from TRIMCyp restriction but not TRIM5α restriction as observed for the other HIV-1mt clones. While CA-Q110D contributed to neither endowment of further resistance to TRIMCyp nor evasion from TRIM5α restriction, CA-Q110D did lead to enhanced single-cycle infectivity to a macaque cell line compared with the other HIV-1mt clones. Our results here indicate that CA-Q110D accelerates viral growth in macaque cells independently of TRIM5 proteins restriction.

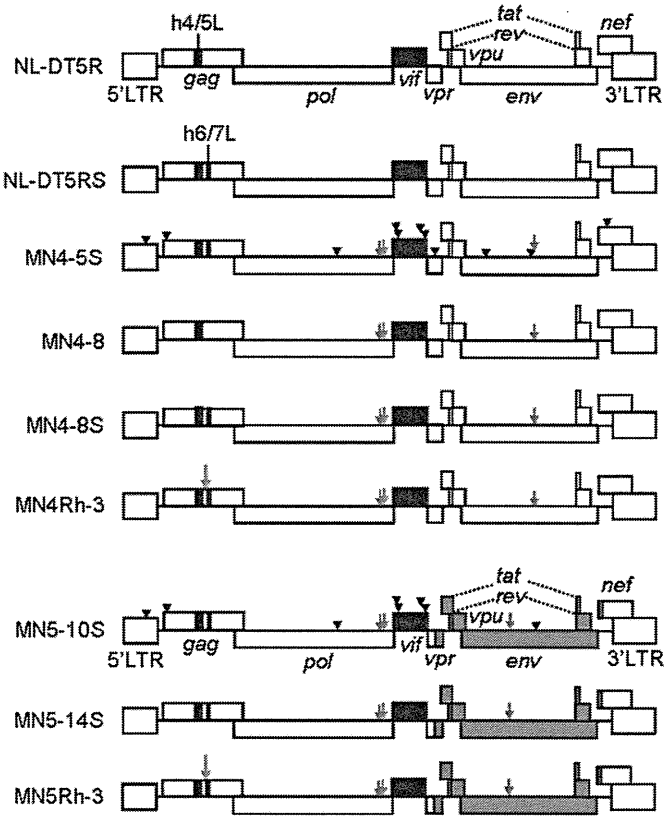

Fig. 1. Proviral genome structure of various HIV-1mt clones used in this study. HIV-1 NL4-3 [26] and SIVmac239 (GenBank: M33262) sequences are indicated by white and black areas, respectively. Gray areas in MN5-10S, MN5-14S and MN5Rh-3 show sequences from NF462 [21]. Blue arrows and black arrowheads show nucleotide substitutions that appeared in viral genomes of NL-DT5R and NL-DT562 during adaptation in HSC-F cells. Among nucleotide substitutions, adaptive mutations that enhance viral growth potential are indicated by blue arrows. Red arrows show the CA-Q110D mutation.

2. Materials and methods

2.1. Plasmid DNA

Construction of NL-DT5R, NL-DT562, NL-DT5RS, and MN4-5S were described previously [16,19–21]. MN4-5S carries all nucleotide substitutions that are present in adapted NL-DT5R and NL-DT562 clones except for mutations in the *env* gene of R5-tropic viruses (MN5-10S, MN5-14S, and MN5Rh-3 in Fig. 1) [19]. MN4-8S contains adaptive (growth-enhancing) mutations in MN4-5S but not the other mutations. MN4Rh-3 was constructed by introduction of the CA-Q110D mutation into MN4-8S. To construct R5-tropic viruses, 3′ halves of viral genomes (*Eco*RI in *vpr* to *Sph*I at the 3′ end of viral genome) of MN4-5S, MN4-8S, and MN4Rh-3 were replaced with the corresponding regions of adapted-NL-DT562,

and were designated MN5-10S, MN5-14S, and MN5Rh-3, respectively. For single-cycle infectivity assays to monitor viral susceptibility to TRIM5 proteins and to determine infectivity for CyM cells, *env*-deficient HIV-1mt variants encoding luciferase gene were constructed. NL-DT5R was cleaved with *Nde*I and *Nhe*I (both sites in *env* gene), blunt ended by T4 DNA polymerase, and resealed by T4 DNA ligase. The resultant clone was designated 5RΔEnv. Luciferase gene was then introduced into *nef* gene of 5RΔEnv as described previously [22], and the resultant clone was designated 5RΔEnv + Luc. A fragment containing the 3′ half genome was cut out from the 5RΔEnv + Luc, and introduced into the corresponding region in HIV-1mt variants (DT5R/4-3, NL-DT5RS, MN4-8, MN4-8S, and MN4Rh-3) to generate 5R/4-3ΔEnv + Luc, 5RSΔEnv + Luc, 4-8ΔEnv + Luc, 4-8SΔEnv + Luc, and 4Rh-3ΔEnv + Luc, respectively.

2.2. Cell culture

A human monolayer cell line 293T [23], a feline kidney cell line CRFK (ATCC CCL-94), and a CyM kidney cell line MK.P3(F) (JCRB 0607) were maintained in Eagles's minimal essential medium (MEM) containing 10% heat-inactivated fetal bovine serum (hiFBS). CRFK cells expressing TRIM5α/TRIMCyp were maintained in MEM containing 10% hiFBS and 400 μg/mL G418 (SIGMA). Macaque lymphocyte cell lines, HSC-F [24] and HSR5.4 [25], were maintained in RPMI-1640 medium containing 10% hiFBS. Recombinant human IL-2 (AbD Serotec) was added to the medium (50 units/mL) for maintenance of HSR5.4 cells. A human lymphocyte cell line MT4/CCR5 (MT4 cells stably expressing CCR5) was maintained in RPMI-1640 medium containing 10% hiFBS and 200 μg/mL hyglomycine (SIGMA).

2.3. Virus replication assays

Virus stocks for infection were prepared from 293T cells transfected with proviral clones as described previously [16,19,26]. Virion-associated reverse transcriptase (RT) activity was measured as described previously [16]. HSC-F cells (10^6) were infected with equal RT units of viruses in the presence of IL-2. For infection of MT4/CCR5 cells (10^6), the spinoculation method [27] was used. Viral growth was monitored by RT activity released into the culture supernatants. We assessed the viral growth potential by the peak day of virus production, and if the viral growth kinetics are similar, by the production level on the peak day.

2.4. Generation and characterization of adapted viral clones

MN4-5S and MN5-10S viruses (Fig. 1) prepared from transfected 293T cells were inoculated into HSR5.4 cells (3×10^6) with an equal amount of viruses (5×10^7 RT units). The cultures were maintained in the presence of IL-2, and HSC-F cells were added on day 34 post-infection. The culture supernatants (collected on day 18 post-cocultivation, the peak day of virus production) were inoculated into fresh HSR5.4 cells, and total DNA was extracted from the cells on day 15 post-infection. Integrated proviruses were amplified from total DNA as two overlapping fragments by the polymerase chain reaction (PCR), and amplified products were cloned into MN5-10S as described previously [16]. Viruses were prepared from 293T cells transfected with the resultant clones, and inoculated into HSR5.4 cells. Only one clone exhibited a rapid growth kinetics compared to MN5-10S, and was designated Ad clone-25. To identify an adaptive mutation that enhances growth potential, each mutation found in the genome of Ad clone-25 was introduced into MN5-14S by site-directed mutagenesis (STRATAGENE). For screening, viruses prepared from transfected 293T cells were inoculated into HSC-F cells, and virus replication was monitored by RT activity released into the culture supernatants.

2.5. Molecular modeling of HIV CA N-terminal domain (NTD)

The crystal structure of HIV-1 CA NTD at a resolution of 2.00 Å (PDB code: 1M9C [28]) was taken from the RCSB Protein Data Bank [29]. The three-dimensional (3-D) models of HIV-1 CA NTD were constructed by the homology modeling technique using 'MOE-Align' and 'MOE-Homology' in the Molecular Operating Environment (MOE) (Chemical Computing Group Inc., Quebec, Canada) as described [30–32]. We obtained 25 intermediate models per one homology modeling in MOE, and selected the 3-D models which were the intermediate models with best scores according to the generalized Born/volume integral methodology [33]. The final 3-D models were thermodynamically optimized by energy minimization using an AMBER99 force field [34] combined with the generalized Born model of aqueous solvation implemented in MOE [35]. Physically unacceptable local structures of the optimized 3-D models were further refined on the basis of evaluation by the Ramachandran plot using MOE.

2.6. Single-cycle infectivity assays

To generate CRFK cells expressing CyM TRIMCyp, the cDNA was isolated from HSC-F cells, and expression vector of FLAG-tagged CyM TRIMCyp was constructed as described previously [18]. The sequence of TRIMCyp from HSC-F cells was identical with Mafa TRIMCyp2 (GenBank: FJ609415). CRFK cell lines expressing CyM TRIMCyp were selected by G418 as described previously [18]. Expression and inhibitory effect of the selected cell clones were verified by Western blotting with anti-FLAG antibody (SIGMA) and by infection with vesicular stomatitis virus G protein (VSV-G) pseudotyped 5R/4-3ΔEnv + Luc, respectively. Assays using naïve CRFK, CRFK expressing CyM TRIM5α [18] or CyM TRIMCyp, and MK.P3(F) cells were similarly performed as described previously [36]. VSV-G pseudotyped virus stocks were prepared from 293T cells transfected with individual HIV-1mtΔEnv + Luc clones and pCMV-G (GenBank: AJ318514)

at a molar ratio of 1:1. Naïve CRFK, CRFK expressing TRIM5α/TRIMCyp and MK.P3(F) cells were infected with an equal titer of viruses (to generate approximately 10^7 relative luminescence (RLU) for naïve CRFK cells), and on day 2 post-infection, cells were analyzed for luciferase activity. Assays using recombinant Sendai virus (SeV)-CyM TRIM5α/TRIMCyp expression system were performed as described previously [31].

3. Results

3.1. An adaptive mutation G114E on helix 6 in CA (CA-G114E) enhances viral growth potential in macaque cells

An HIV-1mt variant MN4-5S replicated more slowly than SIVmac239 in macaque cells. In order to improve its growth potential, we carried out virus adaptation in a macaque lymphocyte cell line HSR5.4. Virus adaptation was performed by long-term culture of HSR5.4 cells infected with MN4-5S (X4-tropic) or its R5-tropic version MN5-10S (Fig. 1). Construction of proviral clones from adapted viruses was described in Materials and methods. We obtained only one clone (Ad clone-25) with enhanced growth potential from 100 proviral clones constructed and tested. We sequenced the entire genome of Ad clone-25, and found three non-synonymous mutations in CA (S33N, G114E, and T147A in Fig. 2A) and one synonymous mutation in integrase (IN)(a4943c in Fig. 2A). To identify an adaptive mutation that enhances growth potential, each mutation found in Ad clone-25 was introduced into a parental clone MN5-14S (Fig. 1). MN5-14S carries only growth-promoting mutations in MN5-10S, and the two clones exhibit similar growth potential in macaque cells. Viruses were prepared from 293T cells transfected with MN5-14S, Ad clone-25, or clones carrying individual mutations, and inoculated into HSC-F cells (Fig. 2A). Only one clone carrying CA-G114E exhibited similar growth kinetics to that of Ad clone-25 but not the others. This result indicates that CA-G114E is an adaptive mutation enhancing growth potential of HIV-1mt in macaque cells. This mutation is exactly the same as the previously found adaptive mutation, which enhanced growth of NL-4/5S6/7SvifS virus in human CEM-SS cells [37]. NL-4/5S6/7SvifS virus is a prototype HIV-1mt bearing the same CA with that of MN4-5S.

3.2. Molecular modeling of the CA NTD of HIV-1mt variants suggests that CA-G114E and CA-Q110D mutations have a similar positive effect on viral replication

The amino acid at position 114 is located in CA NTD. To obtain structural insights into impacts of the G114E substitution in order to improve growth capability of HIV-1mt variants in macaque cells, we conducted computer-assisted structural study: we constructed 3-D models of CA NTD of three HIV-1mt variants, CA-G114E, CA-G114Q, and MN4-5S, using homology-modeling technique (see Materials and methods). Main chain folds of the three models were indistinguishable, suggesting that 3-D position and type of side chain are critical

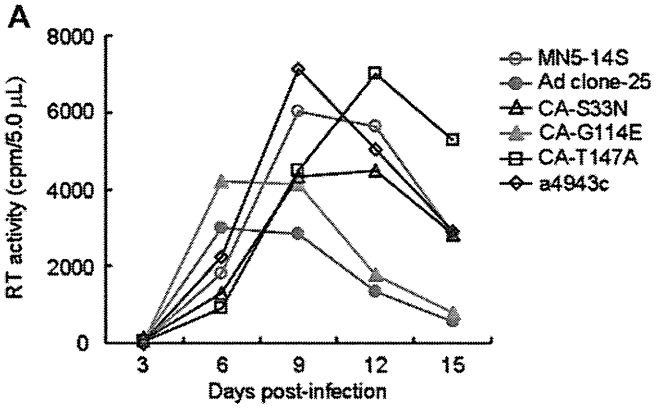

Nucleotide change	Region	Amino acid change in the region
g1283a	CA	S33N
g1526a	CA	G114E
a1624g	CA	T147A
a4943c	IN	None

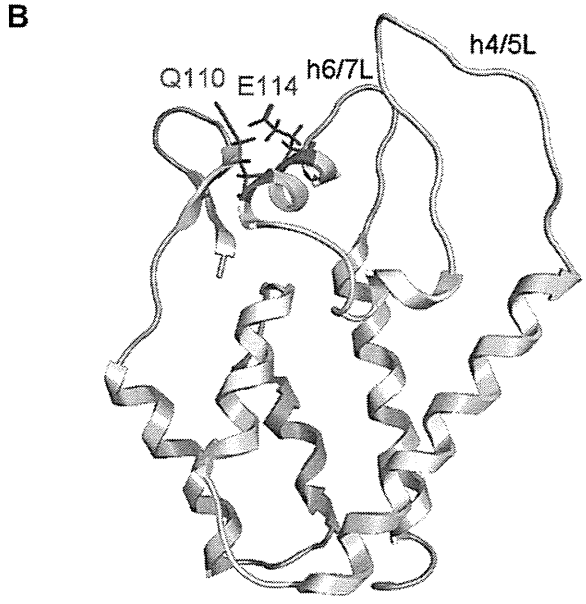

Fig. 2. Mutations in Gag-CA. (A) Identification of an adaptive mutation that enhances viral growth. Nucleotide substitutions found in the genome of Ad clone-25 are indicated at the bottom. Virus samples were prepared from 293T cells transfected with the indicated proviral clones, and equal RT units were inoculated into HSC-F cells. MN5-14S and Ad clone-25 served as controls. Virus replication was monitored by RT activity released into the culture supernatants. (B) 3-D structural models for CA NTD of HIV-1mt variants. Structural models of CA NTD of HIV-1mt variants were constructed by homology-modeling using "MOE-Align" and "MOE-Homology" in MOE as described previously [30–32]. Crystal structure of HIV-1 CA NTD at a resolution of 2.00 Å (PDB code: 1M9C [28]) was used as template for homology modeling. Main chain folds were indistinguishable among the models, and only the model of G114E CA is shown as a representative. Magenta and red sticks: side chains of 110th and 114th amino acid residues, respectively, of the G114E CA NTD.

for the phenotypic change. The modeling study revealed that 114th residue of G114E CA NTD is located on helix 6 in CA NTD such that its side chain protrudes into the exposed surface of CA (Fig. 2B). A charged amino acid residue on a protein surface participates in determining physicochemical properties of interaction surface of the protein and thus influences its structural and functional properties. Therefore, we assumed that the protrusion of a negatively charged side chain from helix 6 into exposed surface could have somehow a positive effect on growth capability of the HIV-1mt variants in macaque cells. In this regard, especially worth noting is that 110th amino acid residue on helix 6 of the HIV-1mt variant CAs was positioned on the same helical face with 114th amino acid residue (Fig. 2B). Therefore, we predicted that substitution of glutamine (Q) at position 110 by acidic amino acid such as aspartic acid (D) and glutamic acid (E) may also have a positive effect on growth capability of the HIV-1mt variants in macaque cells as G114E does. SIVmac239 has aspartic acid and glutamine at the positions 110 and 114, respectively.

3.3. CA-Q110D promotes viral growth more efficiently in macaque cells than CA-G114E mutation but its enhancing effect is species-specific

To confirm our prediction described above, CA-Q110D mutation was introduced into MN5-14S (designated MN5Rh-3), and the growth property in HSC-F cells of MN5Rh-3 and a viral clone carrying G114E (CA-G114E in Fig. 2A) was compared. As shown in Fig. 3A, MN5Rh-3 grew better than CA-G114E, indicating that CA-Q110D further accelerates HIV-1mt replication in macaque cells compared with an adaptive CA-G114E mutation. We next constructed an X4-tropic proviral clone carrying the CA-Q110D (designated MN4Rh-3) (Fig. 1), and compared its growth property with MN5Rh-3 in HSC-F cells (Fig. 3B). MN4Rh-3 was found to exhibit higher growth ability than MN5Rh-3, and was therefore used for infection experiments hereafter.

While CypA and TRIM5α have inhibitory effect on HIV-1 replication in macaque cells, CypA promotes HIV-1 infection in human cells and human TRIM5α only weakly inhibits HIV-1 replication [38–40]. Since the CA-Q110D mutation (acquisition of negatively charged side chain), as predicted by structural modeling, could impact on the interaction of HIV-1 CA and its binding factor(s) by altering physicochemical properties of CA binding surface, it can be speculated that CA-Q110D may promote viral replication specifically in macaque cells. Thus, we analyzed the effect of CA-Q110D on viral growth in macaque and human cells. In this experiment, we used HIV-1mt variants (MN4-8, MN4-8S, and MN4Rh-3) that have distinct CA structures (Fig. 1). Viruses prepared from transfected 293T cells were inoculated into macaque HSC-F and human MT4/CCR5 cells, and examined for growth property (Fig. 3C). The introduction of SIVmac239 CA h6/7L (MN4-8S) resulted in enhanced and reduced viral growth in macaque and human cells, respectively, relative to MN4-8. MN4Rh-3 grew clearly better in macaque cells relative to MN4-8 and MN4-8S, but more poorly in human cells than the other twos. These results demonstrate that the CA-Q110D mutation enhances viral replication in a host cell species-specific manner.

3.4. CA-Q110D does not contribute to evasion from CyM TRIM5 proteins restriction

We predicted that the growth enhancement by CA-Q110D may come from the increased resistance to CyM TRIM5 proteins, and therefore examined the susceptibility of HIV-1mt variants to them by two independent assays.

First, assays were performed in feline kidney CRFK cells expressing TRIM5α or TRIMCyp by using VSV-G pseudotyped viruses encoding the luciferase gene (Fig. 4A–C). The sequence differences between HIV-1mt variants reside only in CA and IN (Figs. 1 and 4). Since adaptive mutations in IN contribute to enhancement of virion production but not early replication phase (manuscript in preparation), only the difference in CA affects the relative single cycle infectivity in this assay. A pseudotyped virus 5R/4-3 carries HIV-1 (NL4-3) CA without any modifications and served as negative control. While 5R and 4-8 have an identical CA structure carrying h4/5L from SIVmac239, 5RS and 4-8S have both h4/5L and h6/7L from SIVmac239 CA. 4Rh-3 carries CA-Q110D mutation in addition to h4/5L and h6/7L from SIVmac239 CA. Viral infectivity was measured by luciferase activity in infected cells and presented as RLU. Naïve CRFK and CRFK cells expressing TRIM5α were infected with an equal amount of viruses generating 10^7 RLU in naïve cells. As shown in Fig. 4B, the infectivity of 5R and 4-8 for cells expressing CyM TRIM5α was similar to that of a negative control 5R/4-3. However, higher infectivity was observed for 5RS and 4-8S relative to 5R and 4-8. These results were consistent with previous reports that h4/5L and h6/7L in HIV-1 CA are a part of determinant for TRIM5α restriction [20,36]. The sensitivity of 4Rh-3 to TRIM5α was similar to that of 5RS and 4-8S. This indicates that CA-Q110D did not contribute to increase the resistance to TRIM5α. It has been reported that CyM TRIMCyp has the ability to restrict HIV-1 replication [15]. To examine the susceptibility of HIV-1mt variants to TRIMCyp, we generated feline CRFK cells expressing TRIMCyp, and the cells were infected with pseudotyped viruses as described above. As shown in Fig. 4C, all the clones tested were more resistant to a similar extent to TRIMCyp than the control 5R/4-3. In agreement with a previous study showing that elimination of alanine at position 88 within h4/5L of HIV-1 CA confers the resistance on the virus to TRIMCyp [15], our results indicate that the replacement of HIV-1 CA h4/5L with that of SIVmac239 is sufficient for HIV-1mt to evade from the TRIMCyp restriction. Second, we performed another susceptibility assay using the recombinant SeV expression system. This system assures a very high expression level of target proteins in cells infected with the recombinant SeV. Therefore, the ability of viruses to completely counteract the restriction effect of TRIM5 proteins could be determined by MT4/SeV-TRIM5 expression system. Human MT4 cells were infected with recombinant SeV expressing CyM TRIM5α, TRIMCyp, or SPRY(−)TRIM5, and then super-infected with HIV-1

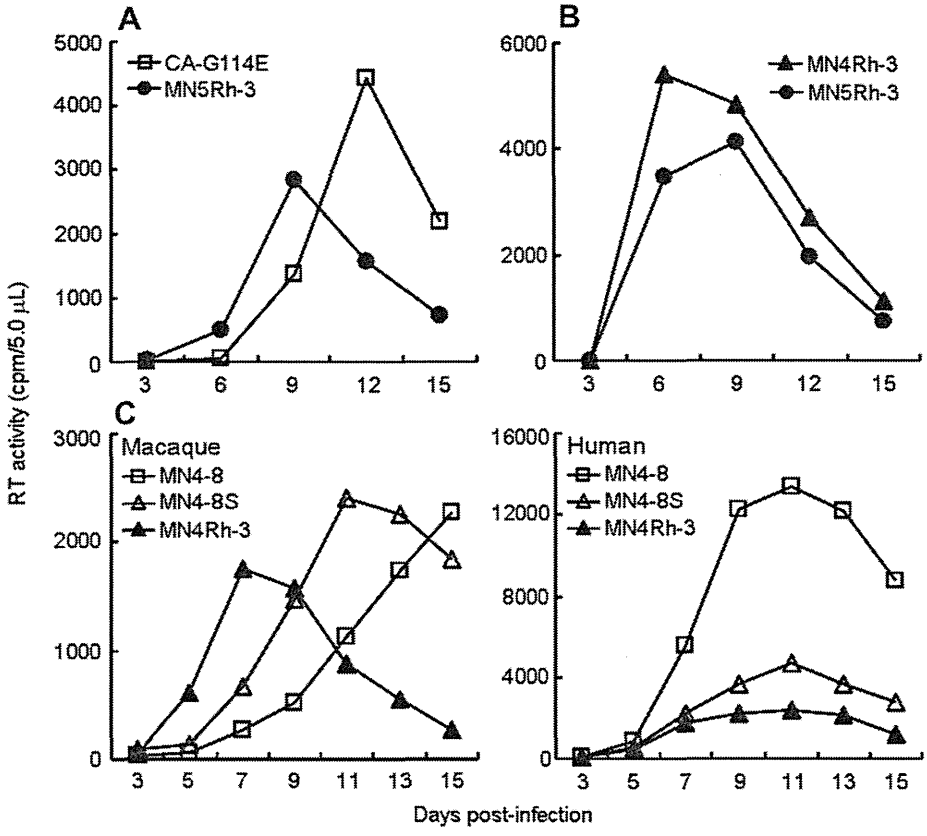

Fig. 3. Effect of CA modification on viral growth in macaque and human lymphocyte cell lines. (A and B) Growth kinetics of HIV-1mt clones carrying CA-G114E or CA-Q110D (MN5Rh-3 and MN4Rh-3) in CyM HSC-F cells. Virus samples were prepared from 293T cells transfected with the indicated proviral clones, and equal amounts (5×10^5 RT units) were inoculated into HSC-F cells (10^6). Virus replication was monitored by RT activity released into the culture supernatants. (C) Growth kinetics of MN4-8, MN4-8S, and MN4Rh-3 in HSC-F (Macaque) and MT4/CCR5 (Human) cells. Virus samples were prepared from 293T cells transfected with the indicated proviral clones, and equal amounts (10^6 RT units) were inoculated into HSC-F cells (10^6). For spinoculation of MT4/CCR5 cells (10^6), 6×10^5 RT units were used as inocula. Virus replication was monitored by RT activity released into the culture supernatants.

(NL4-3), SIVmac239, or HIV-1mt variants. SPRY(−)TRIM5 which can not bind to viral CA served as control. NL4-3 and SIVmac239 also served as controls for viral replication. As shown in Fig. 4D, NL4-3 replicated in cells expressing SPRY(−)TRIM5, but not in TRIM5α and TRIMCyp expressing cells. SIVmac239 exhibited similar growth kinetics in SPRY(−)TRIM5, TRIM5α and TRIMCyp expressing cells. All HIV-1mt variants replicated in TRIMCyp expressing cells similarly well in SPRY(−)TRIM5 cells. Together with assays in CRFK cells, these results showed that all HIV-1mt variants except for 5R/4-3 completely evade from TRIMCyp restriction. In contrast, the growth of all HIV-1mt variants was inhibited in CyM TRIM5α expressing MT4 cells. These results indicate that HIV-1mt variants do not evade from TRIM5α restriction as effectively as SIVmac239.

Results obtained by our two assay systems with respect to the susceptibility of HIV-1mt variants to CyM TRIM5α were apparently different (Fig. 4B and D), but this difference is most likely to be due to the TRIM5α expression level. In MT4 cells infected with recombinant SeV, TRIM5α is expressed at much higher level than that in transduced CRFK cells, masking the increase of resistance to TRIM5α detectable by the transduced CRFK system (Fig. 4B). Indeed, the growth enhancement of 5RS relative to 5R [20] can be explained by the results in Fig. 4B but not those in Fig. 4D. The apparent discrepancy of the sensitivity depending on TRIM5α expression level was also observed between B-LCL cells and transduced CRFK cells [41]. In sum, we can conclude here that MN4Rh-3 exhibits a partial resistance to TRIM5α insufficient for complete evasion as 5RS and 4-8S do, and that the CA-Q110D mutation is irrelevant to this property.

3.5. CA-Q110D enhances viral infectivity for macaque cells

Results so far showed that CA-Q110D does not contribute to evasion from TRIM5 proteins restriction in rather artificial systems using feline and human cells (Fig. 4). To investigate further how CA-Q110D enhances viral replication, we examined single-cycle viral infectivity in macaque cells. CyM kidney MK.P3(F) cells, which have heterozygote for TRIM5α and TRIMCyp, were infected with various VSV-G pseudoviruses and analyzed for their infectivity as described above. As shown in Fig. 5A, viral infectivity was increased by modification of h4/5L (compare 5R/4-3 and 5R&4-8). Modification of h6/7L in addition to h4/5L further augmented viral infectivity (compare 5R&4-8 and 5RS&4-8S). Introduction of the CA-Q110D mutation into 4-8S clone gave the highest infectivity among the viruses tested (see 4Rh-3). The results in

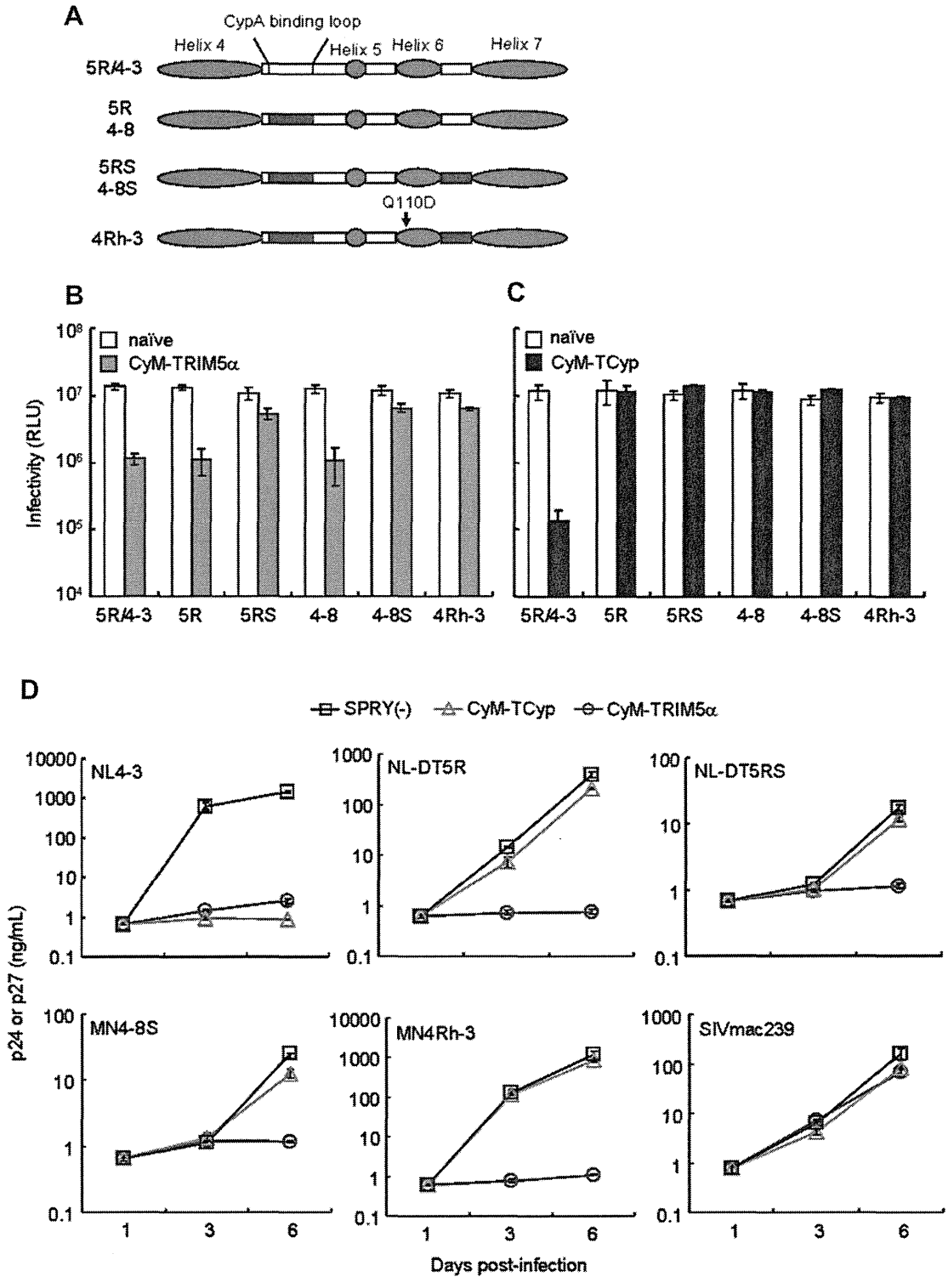

Fig. 4. Effect of CA modification in HIV-1mt variants on viral infectivity. (A) CA structure of viral clones used in TRIM5α/TRIMCyp susceptibility assays. Blue and white areas show helices and loops from HIV-1 NL4-3 CA, respectively. Sequences from SIVmac239 are indicated by black areas. (B and C) Susceptibility of HIV-1mt variants to CyM TRIM5 proteins as examined by CRFK system. Results for CyM TRIM5α (B) and for CyM TRIMCyp (TCyp) (C) are shown. VSV-G pseudotyped viruses were prepared from transfected 293T cells as input samples. Viruses generating 10^7 RLU in CRFK-naïve cells were inoculated into CRFK cells that express CyM TRIM5α or CyM TCyp. On day 2 post-infection, cells were analyzed for luciferase activity by a luminometer. (D) Susceptibility of HIV-1mt variants to CyM TRIM5 proteins as examined by SeV system. Human MT4 cells (10^5) were infected with recombinant SeV expressing CyM TRIM5α, TRIMCyp, or SPRY (−) TRIM5. Nine hours after infection, cells were super-infected with 20 ng (Gag-p24) of HIV-1 NL4-3, various HIV-1mt clones, or 20 ng (Gag-p27) of SIVmac239. Virus replication was monitored by the amount of Gag-p24 from NL4-3 and HIV-1mt clones or Gag-p27 from SIVmac239 in the culture supernatants. Error bars show actual fluctuations between duplicate samples. Data from one representative of three independent experiments are shown.

Fig. 5A show that CA-Q110D uniquely increases viral infectivity in macaque cells not observed in the other experimental systems (Fig. 4), and suggest that some factor(s) in CyM cells other than TRIM5α and TRIMCyp proteins is associated with this enhancement.

As shown in Fig. 5B, MN4Rh-3 displayed slower growth kinetics relative to those of SIVmac239 (note the peak day of virus production), although it grew better than the other HIV-1mt clones in CyM HSC-F cells. Approximately 100-fold more input virus (RT units) compared to SIVmac239 was required for MN4Rh-3 to exhibit similar growth kinetics with SIVmac239 (data not shown). These results have shown that even MN4Rh-3 grows more poorly in macaque cells than a standard SIVmac clone pathogenic for macaque monkeys.

4. Discussion

In this study, we have demonstrated that a single CA mutation (Q110D) greatly promotes HIV-1mt growth in macaque cells (Fig. 3). This enhancing effect was afforded independently of TRIM5 proteins restriction. The virus carrying the CA-Q110D mutation (MN4Rh-3) certainly overcame the anti-viral action of CyM TRIMCyp but not completely CyM TRIM5α. However, the mutation itself (Fig. 1) did not influence anti-TRIMCyp/TRIM5α activity of MN4Rh-3 reported here (Fig. 4). Notably, this mutation exquisitely enhanced viral growth in macaque cells (Fig. 3) by augmenting viral single-cycle infectivity (Fig. 5). The viral growth enhancement reported here is well reproduced in CyM peripheral blood mononuclear cells and in CyMs (manuscript in preparation).

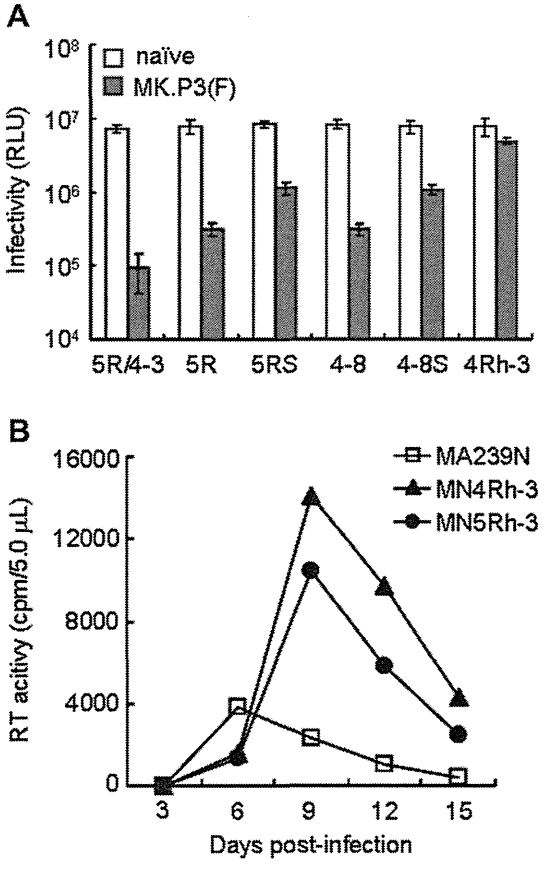

Fig. 5. Replication ability of various viruses in CyM cells. (A) Single-cycle infectivity of various HIV-1mt clones in CyM kidney MK.P3(F) cells. VSV-G pseudotyped viruses indicated were prepared from transfected 293T cells. MK.P3(F) cells were infected with an equal titer of viruses giving 10^7 RLU in CRFK-naïve cells. On day 2 post-infection, cells were analyzed for luciferase activity by a luminometer. (B) Multi-cycle growth kinetics of SIVmac and HIV-1mt viruses in CyM lymphocyte HSC-F cells. Virus samples were prepared from 293T cells transfected with the indicated proviral clones, and equal amounts (10^4 RT units) were inoculated into HSC-F cells (10^6). Virus replication was monitored by RT activity released into the culture supernatants. MA239N, an infectious clone of SIVmac239 with *nef*-open.

Regarding the mechanism for enhancement of viral growth by CA-Q110D, we initially thought a possibility that CA-Q110D compensates the disadvantage in HIV-1mt genome resulted from replacement of HIV-1 CA h4/5L and h6/7L with those of SIVmac239. However, this is highly unlikely because the enhancing effect is macaque cell-dependent (Fig. 3). Most feasible explanation is that CA-Q110D contributes to evade from a negative factor(s) in macaque cells such as CypA. Because HIV-1mt CA was designed not to bind to CypA, and the interaction between the two molecules was indeed undetectable by monitoring CypA virion-incorporation [18,20], we analyzed the binding by computer-assisted structural modeling. Homology modeling of the CA-CypA complexes was performed based on the crystal structure of HIV-1 CA NTD bound to CypA (PDB code: 1M9C [28]), and the binding energies, E_{bind}, were calculated using MOE as described previously [42,43]. As shown in Fig. 6, HIV-1 (NL4-3) CA was predicted to interact with CypA via its h4/5L (binding energy: −64.4 kcal/mol). The binding energy of CA and CypA was decreased by CA modifications, such as h4/5L replacement (NL-DT5R: −31.0 kcal/mol), h4/5L and h6/7L replacement (NL-DT5RS: −36.1 kcal/mol), and Q110D substitution in addition to h4/5L and h6/7L replacement (MN4Rh-3: −30.1 kcal/mol). Decrease in E_{bind} in NL-DT5R is consistent with the result that the h4/5L region directly interacts with CypA [28]. Notably, the E_{bind} for the NL-DT5RS CA was greater than that of the NL-DT5R and MN4Rh-3 CAs. These results suggest that not only h6/7L replacement but also Q110D substitution can influence structure of CypA binding surface of CA. The Q110D substitution is located on the exposed surface of helix 6 connecting to the h6/7L (Fig. 2B). CA helix 6 has been reported to interact with CypA binding region on h4/5L through hydrogen bonding [44,45]. Thereby it is reasonable that the local electrostatic change on the helix 6 by the Q110D substitution influenced structures of h4/5L via changes in fluctuation and conformation of h6/7L. This in turn could lead to reduction in stability of the MN4Rh-3 CA-CypA complex compared with NL-DT5RS CA-CypA complex, as predicted in Fig. 6. Our computer-assisted structural study suggests that the Q110D substitution can induce electrostatic modulation of the overall CA surface structure including h4/5L and h6/7L. Similar modulation mechanism of binding surface structures via charged amino acid substitution at distant site from the binding surface has been reported for Cyp domain of CyM TRIMCyp [15] and CD4 binding site of HIV-1 gp120 outer

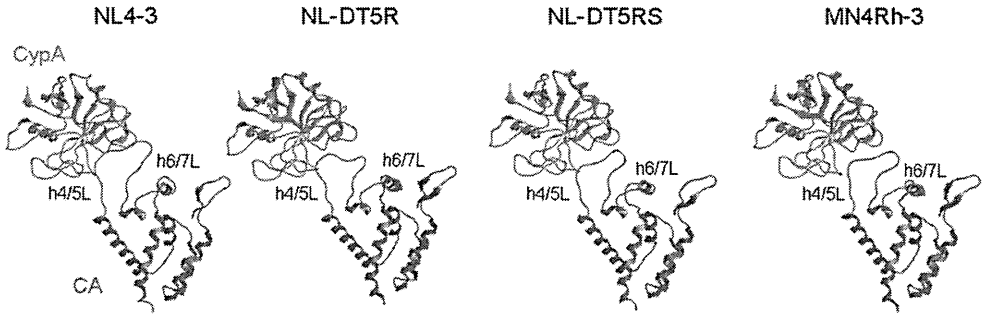

	NL4-3	NL-DT5R	NL-DT5RS	MN4Rh-3
CA	HIV-1 CA	h4/5L from SIVmac239	h4/5L and h6/7L from SIVmac239	h4/5L and h6/7L from SIVmac239 and Q110D
Binding energy (kcal/mol)	-64.447	-31.012	-36.071	-30.051

Fig. 6. Structural models of HIV CA NTD bound to CypA. The model of CA NTD bound to CypA was constructed by homology modeling using the crystal structure of HIV-1 CA NTD and CypA complex (PDB code: 1M9C [28]). The binding energies, E_{bind} (kcal/mol), of the complex were calculated using MOE as described previously [42,43]. The formula $E_{bind} = E_{complex} - (E_{CA} + E_{CypA})$ was used for the E_{bind} calculation, where $E_{complex}$ is the energy of the CA/CypA complex models, E_{CA} is the energy of the CA monomer model, and E_{CypA} is the energy of the CypA monomer model.

domain [46]. Thus, it is not unreasonable to assume that the replication of MN4Rh-3 carrying CA-Q110D is enhanced in macaque cells but reduced in human cells by augmenting its dissociation from CypA (Fig. 6). However, it was found to be difficult to experimentally confirm this structural insight by determining the effect of cyclosporine A or of siRNA against CypA on viral infectivity because interaction between the HIV-1mt CA and CypA was so weak. Alternatively, CA-Q110D may contribute to the alteration of the affinity to unknown anti-CA factor(s) other than CypA and TRIM5 proteins. In this case, it is speculated that the factor(s) might act negatively on HIV-1 replication in macaque cells but positively in human cells, and vice versa. Further study is required to elucidate the mechanism for enhancement of viral growth potential by CA-Q110D.

In conclusion, further modification of the HIV-1mt genome is necessary to overcome unconquered replication block(s) present in macaque cells and obtain viral clones similarly replication-competent in macaque cells and pathogenic for animals with SIVmac (Fig. 5). Considering the genome structure of MN4Rh-3 and the results presented here, major targets for modification now are *gag*-CA (against TRIM5α) and *vpu* (against tetherin). Gag-CA is one of the two principal viral determinants (CA and Vif) for the HIV-1 species-tropism. Construction of HIV-1 CA that evades from TRIM5α restriction is also useful for elucidation of the less-defined CA-TRIM5α interaction and antiviral mechanism of TRIM5α. Tetherin, identified as anti-virion release factor, is antagonized by Vpu [47,48], but macaque tetherin was not counteracted by HIV-1 Vpu [49]. Construction of HIV-1 Vpu that down-modulate macaque tetherin may enhance viral replication *in vivo* as well as *in vitro* [50]. Through these approaches, we may be able to precisely analyze HIV-1 replication and pathogenesis *in vivo* and provide new strategies against HIV-1/AIDS.

Acknowledgments

This study was supported by a grant from the Ministry of Health, Labor and Welfare of Japan (Research on HIV/AIDS project no. H23-003).

References

[1] M.H. Malim, M. Emerman, HIV-1 accessory proteins–ensuring viral survival in a hostile environment, Cell Host Microbe 3 (2008) 388–398.
[2] F. Kirchhoff, Immune evasion and counteraction of restriction factors by HIV-1 and other primate lentiviruses, Cell Host Microbe 8 (2010) 55–67.
[3] R. Shibata, H. Sakai, M. Kawamura, K. Tokunaga, A. Adachi, Early replication block of human immunodeficiency virus type 1 in monkey cells, J. Gen. Virol. 76 (1995) 2723–2730.
[4] M. Nomaguchi, N. Doi, K. Kamada, A. Adachi, Species barrier of HIV-1 and its jumping by virus engineering, Rev. Med. Virol. 18 (2008) 261–275.
[5] M. Nomaguchi, A. Adachi, Virology as biosystematics: towards understanding the viral infection biology, Front. Microbiol. 1 (2010) 2.
[6] R.K. Holmes, M.H. Malim, K.N. Bishop, APOBEC-mediated viral restriction: not simply editing? Trends Biochem. Sci. 32 (2007) 118–128.
[7] H. Huthoff, G.J. Towers, Restriction of retroviral replication by APOBEC3G/F and TRIM5alpha, Trends Microbiol. 16 (2008) 612–619.
[8] K. Strebel, J. Luban, K.T. Jeang, Human cellular restriction factors that target HIV-1 replication, BMC Med. 7 (2009) 48.
[9] J. Luban, Cyclophilin A, TRIM5, and resistance to human immunodeficiency virus type 1 infection, J. Virol. 81 (2007) 1054–1061.
[10] G.J. Towers, The control of viral infection by tripartite motif proteins and cyclophilin A, Retrovirology 4 (2007) 40.
[11] E.E. Nakayama, T. Shioda, Anti-retroviral activity of TRIM5 alpha, Rev. Med. Virol. 20 (2010) 77–92.
[12] R.M. Newman, L. Hall, M. Connole, G.L. Chen, S. Sato, E. Yuste, W. Diehl, E. Hunter, A. Kaur, G.M. Miller, W.E. Johnson, Balancing selection and the evolution of functional polymorphism in old world monkey TRIM5alpha, Proc. Natl. Acad. Sci. U. S. A. 103 (2006) 19134–19139.
[13] S.J. Wilson, B.L. Webb, L.M. Ylinen, E. Verschoor, J.L. Heeney, G.J. Towers, Independent evolution of an antiviral TRIMCyp in rhesus macaques, Proc. Natl. Acad. Sci. U. S. A. 105 (2008) 3557–3562.

[14] A.J. Price, F. Marzetta, M. Lammers, L.M. Ylinen, T. Schaller, S.J. Wilson, G.J. Towers, L.C. James, Active site remodeling switches HIV specificity of antiretroviral TRIMCyp, Nat. Struct. Mol. Biol. 16 (2009) 1036–1042.

[15] L.M. Ylinen, A.J. Price, J. Rasaiyaah, S. Hué, N.J. Rose, F. Marzetta, L.C. James, G.J. Towers, Conformational adaptation of Asian macaque TRIMCyp directs lineage specific antiviral activity, PLoS Pathog. 6 (2010) e1001062.

[16] K. Kamada, T. Igarashi, M.A. Martin, B. Khamsri, K. Hatcho, T. Yamashita, M. Fujita, T. Uchiyama, A. Adachi, Generation of HIV-1 derivatives that productively infect macaque monkey lymphoid cells, Proc. Natl. Acad. Sci. U. S. A. 103 (2006) 16959–16964.

[17] T. Igarashi, R. Iyengar, R.A. Byrum, A. Buckler-White, R.L. Dewar, C.E. Buckler, H.C. Lane, K. Kamada, A. Adachi, M.A. Martin, Human immunodeficiency virus type 1 derivative with 7% simian immunodeficiency virus genetic content is able to establish infections in pig-tailed macaques, J. Virol. 81 (2007) 11549–11552.

[18] K. Kamada, T. Yamashita, K. Hatcho, A. Adachi, M. Nomaguchi, Evasion from CypA- and APOBEC-mediated restrictions is insufficient for HIV-1 to efficiently grow in simian cells, Microbes Infect. 11 (2009) 164–171.

[19] A. Saito, M. Nomaguchi, S. Iijima, A. Kuroishi, T. Yoshida, Y.J. Lee, T. Hayakawa, K. Kono, E.E. Nakayama, T. Shioda, Y. Yasutomi, A. Adachi, T. Matano, H. Akari, Improved capacity of a monkey-tropic HIV-1 derivative to replicate in cynomolgus monkeys with minimal modifications, Microbes Infect. 13 (2011) 58–64.

[20] A. Kuroishi, A. Saito, Y. Shingai, T. Shioda, M. Nomaguchi, A. Adachi, H. Akari, E.E. Nakayama, Modification of a loop sequence between alpha-helices 6 and 7 of virus capsid (CA) protein in a human immunodeficiency virus type 1 (HIV-1) derivative that has simian immunodeficiency virus (SIVmac239) vif and CA alpha-helices 4 and 5 loop improves replication in cynomolgus monkey cells, Retrovirology 6 (2009) 70.

[21] T. Yamashita, N. Doi, A. Adachi, M. Nomaguchi, Growth ability in simian cells of monkey cell-tropic HIV-1 is greatly affected by downstream region of the vif gene, J. Med. Invest. 55 (2008) 236–240.

[22] M. Yamashita, M. Emerman, Capsid is a dominant determinant of retrovirus infectivity in nondividing cells, J. Virol. 78 (2004) 5670–5678.

[23] J.S. Lebkowski, S. Clancy, M.P. Calos, Simian virus 40 replication in adenovirus-transformed human cells antagonizes gene expression, Nature 317 (1985) 169–171.

[24] H. Akari, T. Fukumori, S. Iida, A. Adachi, Induction of apoptosis in herpesvirus saimiri-immortalized T lymphocytes by blocking interaction of CD28 with CD80/CD86, Biochem. Biophys. Res. Commun. 263 (1999) 352–356.

[25] N. Doi, S. Fujiwara, A. Adachi, M. Nomaguchi, Growth ability in various macaque cell lines of HIV-1 with simian cell-tropism, J. Med. Invest. 57 (2010) 284–292.

[26] A. Adachi, H.E. Gendelman, S. Koenig, T. Folks, R. Willey, A. Rabson, M.A. Martin, Production of acquired immunodeficiency syndrome-associated retrovirus in human and nonhuman cells transfected with an infectious molecular clone, J. Virol. 59 (1986) 284–291.

[27] U. O'Doherty, W.J. Swiggard, M.H. Malim, Human immunodeficiency virus type 1 spinoculation enhances infection through virus binding, J. Virol. 74 (2004) 10074–10080.

[28] B.R. Howard, F.F. Vajdos, S. Li, W.I. Sundquist, C.P. Hill, Structural insights into the catalytic mechanism of cyclophilin A, Nat. Struct. Biol. 10 (2003) 475–481.

[29] N. Deshpande, K.J. Addess, W.F. Bluhm, J.C. Merino-Ott, W. Townsend-Merino, Q. Zhang, C. Knezevich, L. Xie, L. Chen, Z. Feng, R.K. Green, J.L. Flippen-Anderson, J. Westbrook, H.M. Berman, P.E. Bourne, The RCSB protein data bank: a redesigned query system and relational database based on the mmCIF schema, Nucleic Acids Res. 33 (Database issue) (2005) D233–D237.

[30] H. Song, E.E. Nakayama, M. Yokoyama, H. Sato, J.A. Levy, T. Shioda, A single amino acid of the human immunodeficiency virus type 2 capsid affects its replication in the presence of cynomolgus monkey and human TRIM5alphas, J. Virol. 81 (2007) 7280–7285.

[31] K. Kono, H. Song, M. Yokoyama, H. Sato, T. Shioda, E.E. Nakayama, Multiple sites in the N-terminal half of simian immunodeficiency virus capsid protein contribute to evasion from rhesus monkey TRIM5α-mediated restriction, Retrovirology 7 (2010) 72.

[32] N. Inagaki, H. Takeuchi, M. Yokoyama, H. Sato, A. Ryo, H. Yamamoto, M. Kawada, T. Matano, A structural constraint for functional interaction between N-terminal and C-terminal domains in simian immunodeficiency virus capsid proteins, Retrovirology 7 (2010) 90.

[33] P. Labute, The generalized Born/volume integral implicit solvent model: estimation of the free energy of hydration using London dispersion instead of atomic surface area, J. Comput. Chem. 29 (2008) 1693–1698.

[34] J.W. Ponder, D.A. Case, Force fields for protein simulations, Adv. Protein Chem. 66 (2003) 27–85.

[35] A. Onufriev, D. Bashford, D.A. Case, Modification of the generalized Born model suitable for macromolecules, J. Phys. Chem. B 104 (2000) 3712–3720.

[36] T.Y. Lin, M. Emerman, Determinants of cyclophilin A-dependent TRIM5 alpha restriction against HIV-1, Virology 379 (2008) 335–341.

[37] A. Kuroishi, K. Bozek, T. Shioda, E.E. Nakayama, A single amino acid substitution of the human immunodeficiency virus type 1 capsid protein affects viral sensitivity to TRIM5 alpha, Retrovirology 7 (2010) 58.

[38] M. Stremlau, C.M. Owens, M.J. Perron, M. Kiessling, P. Autissier, J. Sodroski, The cytoplasmic body component TRIM5alpha restricts HIV-1 infection in old world monkeys, Nature 427 (2004) 848–853.

[39] Z. Keckesova, L.M. Ylinen, G.J. Towers, Cyclophilin A renders human immunodeficiency virus type 1 sensitive to old world monkey but not human TRIM5 alpha antiviral activity, J. Virol. 80 (2006) 4683–4690.

[40] E. Sokolskaja, L. Berthoux, J. Luban, Cyclophilin A and TRIM5alpha independently regulate human immunodeficiency virus type 1 infectivity in human cells, J. Virol. 80 (2006) 2855–2862.

[41] S.Y. Lim, T. Rogers, T. Chan, J.B. Whitney, J. Kim, J. Sodroski, N.L. Letvin, TRIM5alpha modulates immunodeficiency virus control in rhesus monkeys, PLoS Pathog. 6 (2010) e1000738.

[42] C.O. Onyango, A. Leligdowicz, M. Yokoyama, H. Sato, H. Song, E.E. Nakayama, T. Shioda, T. de Silva, J. Townend, A. Jaye, H. Whittle, S. Rowland-Jones, M. Cotten, HIV-2 capsids distinguish high and low virus load patients in a West African community cohort, Vaccine 28 (2010) B60–B67.

[43] M. Kinomoto, R. Appiah-Opong, J.A. Brandful, M. Yokoyama, N. Nii-Trebi, E. Ugly-Kwame, H. Sato, D. Ofori-Adjei, T. Kurata, F. Barre-Sinoussi, T. Sata, K. Tokunaga, HIV-1 proteases from drug-naive West African patients are differentially less susceptible to protease inhibitors, Clin. Infect. Dis. 41 (2005) 243–251.

[44] R.K. Gitti, B.M. Lee, J. Walker, M.F. Summers, S. Yoo, W.I. Sundquist, Structure of the amino-terminal core domain of the HIV-1 capsid protein, Science 273 (1996) 231–235.

[45] C. Tang, Y. Ndassa, M.F. Summers, Structure of the N-terminal 283-residue fragment of the immature HIV-1 Gag polyprotein, Nat. Struct. Biol. 9 (2002) 537–543.

[46] M. Yokoyama, S. Naganawa, K. Yoshimura, S. Matsushita, H. Sato, Structural dynamics of HIV-1 envelope Gp120 outer domain with V3 loop, PLoS One 7 (2012) e37530.

[47] S.J. Neil, T. Zang, P.D. Bieniasz, Tetherin inhibits retrovirus release and is antagonized by HIV-1 Vpu, Nature 451 (2008) 425–430.

[48] N. Van Damme, D. Goff, C. Katsura, R.L. Jorgenson, R. Mitchell, M.C. Johnson, E.B. Stephens, J. Guatelli, The interferon-induced protein BST-2 restricts HIV-1 release and is downregulated from the cell surface by the viral Vpu protein, Cell Host Microbe 3 (2008) 245–252.

[49] D. Sauter, M. Schindler, A. Specht, W.N. Landford, J. Münch, K.A. Kim, J. Votteler, U. Schubert, F. Bibollet-Ruche, B.F. Keele, J. Takehisa, Y. Ogando, C. Ochsenbauer, J.C. Kappes, A. Ayouba, M. Peeters, G.H. Learn, G. Shaw, P.M. Sharp, P. Bieniasz, B.H. Hahn, T. Hatziioannou, F. Kirchhoff, Tetherin-driven adaptation of Vpu and Nef function and the evolution of pandemic and nonpandemic HIV-1 strains, Cell Host Microbe 6 (2009) 409–421.

[50] M. Shingai, T. Yoshida, M.A. Martin, K. Strebel, Some human immunodeficiency virus type 1 Vpu proteins are able to antagonize macaque BST-2 in vitro and in vivo: Vpu-negative simian-human immunodeficiency viruses are attenuated in vivo, J. Virol. 85 (2011) 9708–9715.

Cleaved/Associated TLR3 Represents the Primary Form of the Signaling Receptor

Florent Toscano,*,[1] Yann Estornes,*,[1] François Virard,* Alejandra Garcia-Cattaneo,† Audrey Pierrot,* Béatrice Vanbervliet,* Marc Bonnin,* Michael J. Ciancanelli,‡ Shen-Ying Zhang,‡,§ Kenji Funami,¶ Tsukasa Seya,¶ Misako Matsumoto,¶ Jean-Jacques Pin,‖ Jean-Laurent Casanova,‡,§,# Toufic Renno,* and Serge Lebecque*

TLR3 belongs to the family of intracellular TLRs that recognize nucleic acids. Endolysosomal localization and cleavage of intracellular TLRs play pivotal roles in signaling and represent fail-safe mechanisms to prevent self-nucleic acid recognition. Indeed, cleavage by cathepsins is required for native TLR3 to signal in response to dsRNA. Using novel Abs generated against TLR3, we show that the conserved loop exposed in LRR12 is the single cleavage site that lies between the two dsRNA binding sites required for TLR3 dimerization and signaling. Accordingly, we found that the cleavage does not dissociate the C- and N-terminal fragments, but it generates a very stable "cleaved/associated" TLR3 present in endolysosomes that recognizes dsRNA and signals. Moreover, comparison of wild-type, noncleavable, and C-terminal–only mutants of TLR3 demonstrates that efficient signaling requires cleavage of the LRR12 loop but not dissociation of the fragments. Thus, the proteolytic cleavage of TLR3 appears to fulfill function(s) other than separating the two fragments to generate a functional receptor. *The Journal of Immunology*, **2013, 190: 764–773.**

Toll-like receptors belong to a family of pattern recognition receptors that sense the presence of pathogens and trigger a protective innate immune response (1). These germline-encoded type I integral membrane glycoproteins bind their ligands through their extracellular domain (ECD), which is composed of 19–25 leucine-rich repeats (LRRs) (2). In contrast with other members of the family that primarily recognize molecular patterns specific for nonself invaders, TLR3, TLR7, and TLR9 recognize nucleic acids originating from microbes, as well as from the host. Several fail-safe mechanisms prevent self-polynucleotide recognition and subsequent autoimmune disorders (3). Ligands must be recognized by cell surface receptor(s) (4) that mediate their internalization before encountering the corresponding TLR exclusively in the acidic endolysosomal compartment from which signal transduction can be initiated (5). Delivery of intracellular TLRs to the endocytic compartments is also tightly regulated by the chaperone Unc93b1 (6, 7). Finally, processing by pH-dependent lysosomal proteases is an additional checkpoint for controlling TLR9 activation (8–10).

Although several studies on intracellular TLRs have been based on TLR9 trafficking and processing, less is known about TLR3. TLR3 appears to be dedicated to the recognition of dsRNA (11), and it plays a central role in the defense against HSV-1 infection in the CNS in humans (12–15). Although endogenous mRNA can activate TLR3 in vitro (16), its involvement in the autoimmune response has not been demonstrated. It was shown that TLR3 dimerization is needed for dsRNA binding and signaling (17). Moreover, analysis of the crystal structure (18, 19) and mutagenesis (18, 20, 21) of TLR3 ECD revealed that dsRNA binding requires interaction of the negatively charged ribose backbone of dsRNA with residues of TLR3 dimers located in LRR1 and LRR3, as well as with a second region formed by LRR19–LRR21 that becomes positively charged in the mildly acidified endolysosomal compartment. Therefore, the requirement for cleavage of the ECD for TLR3 signaling (9, 10, 22) raises an intriguing issue with regard to how endogenous TLR3 is processed and which forms of the receptor recognize dsRNA. In this study, we generated and used novel mAbs directed against TLR3 ECD and mutant forms of TLR3 to demonstrate that cleavage of the LRR12 loop, but not separation of the two fragments, is required for signaling.

Materials and Methods

Cell culture and reagents

HEK293 and HEK293-TLR3-hemagglutinin (HA) cells (InvivoGen) were grown in DMEM medium (Invitrogen) supplemented with 10% FBS and penicillin/streptomycin. Human bronchial epithelial cell line BEAS-2B (Sigma) was cultured in LHC-9 medium (Invitrogen) in bovine collagen

*Centre de Recherche en Cancérologie de Lyon, INSERM Unité Mixte de Recherche 1052/Centre National de la Recherche Scientifique 5286, Centre Léon Bérard, 69008 Lyon, France; †Institut Curie, INSERM U932, 75005 Paris, France; ‡St. Giles Laboratory of Human Genetics of Infectious Diseases, Rockefeller Branch, The Rockefeller University, New York, NY 10065; §Laboratory of Human Genetics of Infectious Diseases, Necker Branch, INSERM U980, University Paris Descartes, Paris 75015, France; ¶Department of Microbiology and Immunology, Graduate School of Medicine, Hokkaido University, Kita-ku, Sapporo 060-8638, Japan; ‖DENDRITICS SAS, Bioparc Laennec, 69008 Lyon, France; and #Pediatric Immunology-Hematology Unit, Necker Hospital for Sick Children, Paris 75015, France

[1]F.T. and Y.E. contributed equally to this work.

Received for publication August 21, 2012. Accepted for publication November 15, 2012.

This work was supported by Cancéropôle Lyon-Auvergne-Rhône-Alpes.

F.T., Y.E., F.V., A.G.-C., M.J.C., S.-Y.Z., T.S., M.M., T.R., and S.L. designed the experiments. F.T., Y.E., F.V., A.G.-C., A.P., B.V., S.-Y.Z., M.J.C., M.B., K.F., and J.-J.P. performed experiments and analyzed data. F.T., Y.E., F.V., J.-L.C., T.R., and S.L. wrote the manuscript, with all authors providing detailed comments and suggestions. S.L. directed the project.

Address correspondence and reprint requests to Prof. Serge Lebecque, Centre de Recherche en Cancérologie de Lyon, INSERM Unité Mixte de Recherche 1052/Centre National de la Recherche Scientifique 5286, Centre Léon Bérard, 28 rue Laennec, 69008 Lyon, France. E-mail address: serge.lebecque@univ-lyon1.fr

The online version of this article contains supplemental material.

Abbreviations used in this article: DC, dendritic cell; ECD, extracellular domain; EEA, early endosome Ag; EndoH, endoglycosidase H; ER, endoplasmic reticulum; FL, full length; HA, hemagglutinin; HMW, high molecular weight; LMW, low molecular weight; LRR, leucine-rich repeat; mDC, monocyte-derived dendritic cell; NSCLC, non-small cell lung cancer; PNGase, peptide:*N*-glycosidase F; Poly(A:U), polyadenylic-polyuridylic acid; Poly(I:C), polyinosinic-polycytidylic acid; siRNA, small interfering RNA; WT, wild-type.

www.jimmunol.org/cgi/doi/10.4049/jimmunol.1202173

type I (Invitrogen) and fibronectin (Sigma)-coated dishes. $CD14^+$ monocytes were purified from peripheral blood of healthy donors: PBMCs were isolated from human peripheral blood by standard density-gradient centrifugation on Pancoll (PAN Biotech) and then mononuclear cells were separated from PBLs on a 50% Percoll solution (GE Healthcare). Monocytes were enriched by one step of adherence and differentiated in immature dendritic cells (DCs) in complete RPMI 1640 medium supplemented with 200 ng/ml human GM-CSF (kind gift of Schering-Plough) and 50 ng/ml human rIL-4 (R&D Systems) for 6 d. NCI-H292 and NCI-H1703 non-small cell lung cancer (NSCLC) cell lines (American Type Culture Collection) were grown in RPMI 1640 medium (Invitrogen) supplemented with 10% FBS (Sigma), HEPES, NaPy, 100 U/ml penicillin/streptomycin, and 2 mM glutamine. THP1 and U937 cell lines were grown in RPMI 1640 medium (Invitrogen) supplemented with 10% FBS and 100 U/ml penicillin/streptomycin. IFN-α was from Schering-Plough. Z-FA-fmk, chloroquine, tunicamycin, and cycloheximide were from Sigma. Polyinosinic-polycytidylic acid [Poly(I:C)]-high molecular weight (HMW) and Poly(I:C)-low molecular weight (LMW) were purchased from InvivoGen. polyadenylic-polyuridylic acid [Poly(A:U)] was from Innate Pharma. Mouse monoclonal IgG1 anti-actin Ab was from MP Biomedicals. Anti-mouse TLR3 Ab T3.7C3 was a gift from Nadège Goutagny (Centre de Recherche sur le Cancer de Lyon, Lyon, France). HRP-conjugated donkey anti-mouse secondary Ab was from Jackson ImmunoResearch.

TLR3.2 and TLR3.3 Ab preparation and purification

BALB/C mice were immunized with recombinant human TLR3 ECD (R&D Systems) by three i.p. injections of the immunogen in the presence of Freund's adjuvant and a final i.v. boost, 3 d before spleen isolation. Splenic cells were fused with the SP20 myeloma cell line in the presence of polyethylene glycol. Hybridoma supernatants were screened by immunofluorescent staining of pUNO-hTLR3-HA and pUNO-hTLR3-V5 transiently transfected 293T cells with Exgen 500 (Euromedex) and fixed with acetone. Only clones recognizing both transfected cells were selected.

Western blotting

Cells were lysed in cold lysis buffer (20 mM Tris-HCl [pH 7.4], 150 mM NaCl, 0.2% Nonidet P-40, supplemented with 1 mM orthovanadate, 10 mM NaF, and a protease inhibitor mixture; Sigma) for 25 min on ice. Cell lysates were cleared by centrifugation (13,000 × *g* for 10 min at 4°C), and protein concentration was determined using the Bradford assay (Bio-Rad). Protein lysates were denatured or not in Laemmli buffer containing 1% SDS and 5 mM DTT and heated to 95°C for 5 min. For peptide:*N*-glycosidase F (PNGase)/endoglycosidase H (EndoH) digestions, lysates were treated as recommended by the manufacturer (New England BioLabs). Proteins were resolved on SDS-polyacrylamide gels and transferred onto polyvinylidene difluoride membranes by electroblotting, and nonspecific binding sites were blocked using TBS containing 0.1% Tween-20 and 5% (w/v) dry milk. After incubation with the appropriate secondary Abs conjugated to HRP, blots were revealed using ECL (GE Healthcare) or SuperSignal (Thermo Scientific) reagents. For reimmunoprecipitation experiments, anti-TLR3 or anti-HA immunoprecipitates were eluted with preheated lysis buffer containing 1% SDS and 5 mM DTT; 20% of each sample was resolved by SDS-PAGE, and the remaining 80% was diluted 10-fold in lysis buffer and then reimmunoprecipitated with TLR3.2 or anti-HA Ab, resolved by SDS-PAGE, and analyzed with either TLR3.2 or TLR3.3 Ab.

Immunofluorescence

Cells were washed with PBS, fixed with 4% formaldehyde for 10 min at room temperature, and washed three times with PBS. Cells were then blocked using Image-iT FX signal enhancer (Life Technologies) for 30 min at room temperature and washed once with PBS. Thereafter, each washing step was done using TBS. Cells were incubated for 1 h at room temperature with TLR3.1, anti-HA, anti-calreticulin, early endosome Ag (EEA)1, or Lamp1 (Abcam) primary Abs. After washing three times, cells were incubated for 30 min at room temperature with secondary Abs (goat anti-mouse–Alexa Fluor 488 and goat anti-rabbit–Alexa Fluor 555 or Alexa Fluor 633; Life Technologies). Cells were washed again 3 min each. Cover slips were air-dried and then mounted using ProLong Gold antifade reagent with DAPI (Life Technologies). Images were acquired using a confocal microscope (Zeiss Axiovert 100 M LSM510) with a 1.4 NA Plan-Apochromat 63× oil-immersion lens. Image noise was reduced using a Despeckle Fiji filter.

Cytokines measurement

The supernatant from NCI-H292 and NCI-H1703 cells, cultured or not with 100 μg/ml Poly(I:C) for 24 h, was assayed for IL-6, IP-10, and RANTES using a MILLIPLEX MAP kit (Millipore) on a Luminex Bio-Plex 200 System Analyzer (Bio-Rad). The supernatant from monocyte-derived DCs (mDCs), cultured or not with 100 μg/ml Poly(I:C) for 24 h, was assayed for IL-6, IP-10, TNF-α, and IFN-λ using a Quantikine ELISA test (R&D Systems), as described by the manufacturer.

DNA cloning

Preparation of the LRR1-11 and 13-21 deletion mutants was described previously (23). For the TLR3-Ins12-HA mutant, mutagenesis was performed using the QuikChange XL Site-Directed Mutagenesis Kit (Stratagene) and primer pairs containing deletion of 24 nucleotides: 5′-CTGAATTTGAAACG-GTCTTTTACTCTCCCCAAGATTGATGATTTTTCT-3′ (forward) and 5′-AGAAAAATCATCAATCTTGGGGAGAGTAAAAGACCGTTTCAAA-TTCAG-3′ (reverse). Ten nanograms of plasmid DNA and 125 ng of primers were used, according to the manufacturer's instructions. Two colonies from each library were sequenced.

For the TLR3-$Cter_{356}$-HA mutant, LRR deletion mutants of TLR3 (A_{22}–K_{356}) were generated by PCR with Phusion (Finnzyme), using the appropriate primers: 5′-TGTTTGGAGCACCTTAACATGGAAG-3′ (forward) and 5′-GGTGGAGGATGCACACAGCATCCCA-3′ (reverse). PCR was performed with the following cycling conditions: 10 s at 98°C, 2 min at 72°C for 25 cycles. The PCR product was treated with DpnI to digest the template DNA, phosphorylated with T4 PNK (New England BioLabs), and ligated using a DNA Ligation kit (New England BioLabs). Deletion constructs were sequenced. TLR3-$Cter_{346}$ was provided by P. Bénaroch (Curie Institute, Paris, France).

RNA interference

Synthetic TRIF (L-012833-00-0005) and control nonsilencing (D-001810-03-20) small interfering RNAs (siRNAs) were from Dharmacon. TLR3 Stealth RNAi siRNA (TLR3HSS110816) was from Invitrogen. siRNAs mix was prepared in Opti-MEM medium (Invitrogen), and cells in suspension were transfected using HiPerFect reagent (QIAGEN), as described by the manufacturer. The final siRNA concentrations were 25 nM. Transfected cells were seeded in 6-well plates or 96-well white plates (Greiner) and incubated for 24 h. Medium was replaced with fresh complete medium, and cells were incubated for 48 h before Poly(I:C) treatment.

Generation of ISRE– and NF-κB–luciferase reporter cell lines

HEK293, NCI-H292, and NCI-H1703 cells were transduced with luciferase ISRE- or NF-κB–reporter lentiviruses (SABiosciences), according to the manufacturer's recommendations, and transduced cells were selected with puromycin.

Reporter luciferase assays

Cells were seeded in white 96-well plates (10,000 cells/well); 24 h later they were treated with 10 μg/ml poly(I:C) in 50 μl medium for 4 or 6 h, depending on the cell line. Then, 50 μl Steady-Glo reactive (Promega) was added to each well before reading luminescence with a Tecan Infinite 200 microplate reader using i-control software (Tecan).

Transient expression in HEK293 cells

Cells were seeded in 100-mm dishes to reach ~70% confluence on the day of transfection. Cells were transfected with pUNO, TLR3–wild-type (WT)-HA, TLR3-Ins12-HA, TLR3-$Cter_{356}$-HA, or TLR3-$Cter_{346}$-HA by incubating 8 μl Lipofectamine 2000 (Invitrogen) with 8 μg plasmid in 6 ml Opti-MEM medium for 5 h; subsequently, Opti-MEM was replaced by fresh medium. Twenty-four hours after transfection, cells were trypsinized and seeded in 96-well white plates and 6-well plates and incubated for 24 h.

Stable transfections

P2.1 cells were transfected with pUNO-hTLR3 vectors, which contain WT TLR3 cDNA, TLR3-Ins12 mutant, or TLR3-Cter356 mutant cDNA, or with an empty mock vector, in the presence of Lipofectamine Reagent (Invitrogen) and PLUS Reagent (Invitrogen), as described by the manufacturer. Stable transfectants were selected with medium containing blasticidin (5 μg/ml; Invitrogen). The presence of TLR3 was confirmed by Western blotting.

Determination of mRNA levels by RT-quantitative PCR

Total RNA was extracted from P2.1 cells. RNA was reverse-transcribed using Oligo-deoxy-thymidine. To determine mRNA levels for IL-29, quantitative PCR was performed with Assays-on-Demand probe/primer combinations and 2× universal reaction mixture in an ABI Prism 7700 Sequence Detection System (all from Applied Biosystems). The β-glucuronidase (GUS) gene was used for normalization. Results are expressed according to the ΔCt method, as described by the manufacturer.

Coimmunoprecipitation

Cells were cultured in 150-mm dishes, collected, washed in PBS, and lysed in 750 μl cold lysis buffer (20 mM Tris-HCl [pH 7.4], 150 mM NaCl, 0.2% Nonidet P-40, supplemented with 1 mM orthovanadate, 10 mM NaF, and a protease inhibitor mixture; Sigma) for 25 min on ice. Cell lysates were cleared by centrifugation (13,000 × *g* for 10 min at 4°C). Lysates were precleared with 50 μl Sepharose-6B (Sigma) for 1 h at 4°C and then immunoprecipitated overnight at 4°C with 5 μg mouse anti-TLR3.2, anti-TLR3.3, or control IgG1 Ab (R&D Systems) and the following day in the presence of 20 μl protein G–Sepharose for 3 h at 4°C. Beads were recovered by centrifugation, and immunoprecipitates were washed extensively with lysis buffer and eluted with Laemmli buffer containing 1% SDS and 5 mM DTT and heated to 95°C for 10 min.

TLR3 ECD modeling

The MacPyMOL software (DeLano Scientific) was used to generate the 3D representation of the TLR3 structure shown on Figs. 1C and 5A (PDB:1ZIW).

Statistical analysis

Statistical significance was determined using the Student *t* test.

Results

Profiling endogenous TLR3 expression

To analyze the biology of endogenous TLR3, we generated three new mAbs (designated as TLR3.1, TLR3.2, and TLR3.3) raised against the ECD of the receptor. First, the Abs were validated using HEK293 cells stably expressing TLR3 tagged with a C-terminal HA epitope (HEK293-TLR3-HA). In this model, Western blots probed with anti-HA, TLR3.2, and TLR3.3 Abs revealed an ~130 kDa band corresponding to the expected molecular mass of highly glycosylated TLR3 (Fig. 1A) (24). The stronger signal observed with TLR3.2 suggested that this Ab has a higher affinity for TLR3 than does TLR3.3. In addition, anti-HA and TLR3.2 Abs stained a second band at ~72 kDa similar to the C-terminal fragment of TLR3 observed after cleavage by cathepsin. In addition, TLR3.3 Ab detected a third band (Fig. 1A) not recognized by anti-HA mAb and with a size ~60 kDa that could represent the N-terminal fragment of cleaved TLR3. TLR3.1 Ab did not detect TLR3 by Western blot, but it showed the same staining by immunofluorescence as observed with anti-HA Ab (Fig. 1B, Supplemental Fig. 1A). To unequivocally identify the different bands revealed by TLR3.2 and TLR3.3 Abs on Western blot, we mapped the recognized epitopes using 20 single LRR-deleted forms of the ECD of TLR3 (LRR1–11 and LRR13–21) (23). Fig. 1C establishes that TLR3.2 Ab recognizes an epitope present in LRR20, whereas TLR3.3 binds to an epitope formed by residues present in LRR7 and LRR8. We next verified whether similar expression profiles could be observed in human cells of different origins and wondered how treatment with IFN-α, which is known to upregulate the expression of TLR3 (25), would modify this pattern. We determined TLR3 expression by immunoblot of lysates from mDCs (Fig. 1D), from human monocytic cell lines U937 and THP1 (Supplemental Fig. 1B, 1C), and from human bronchial epithelial cells transformed by SV40-T Ag (BEAS-2B; Supplemental Fig. 1D) or derived from NSCLC (NCI-H292 and NCI-H1703; Fig. 1E). The three forms of TLR3 (130, 72, and 60 kDa) were present in every lysate with the exception of THP1, which did not appear to express TLR3 (Supplemental Fig. 1B) or respond to Poly(I:C) (Supplemental Fig. 1E). Resting MRC-5 cells were also devoid of TLR3, but kinetic analysis showed that IFN-α treatment led first to the detection of the high molecular mass bands (~130 and ~135 kDa) of TLR3, followed by an increase in the intensity of the lower ~72-kDa molecular mass band detected by TLR3.2 mAb (Fig. 1F), suggesting that the former might

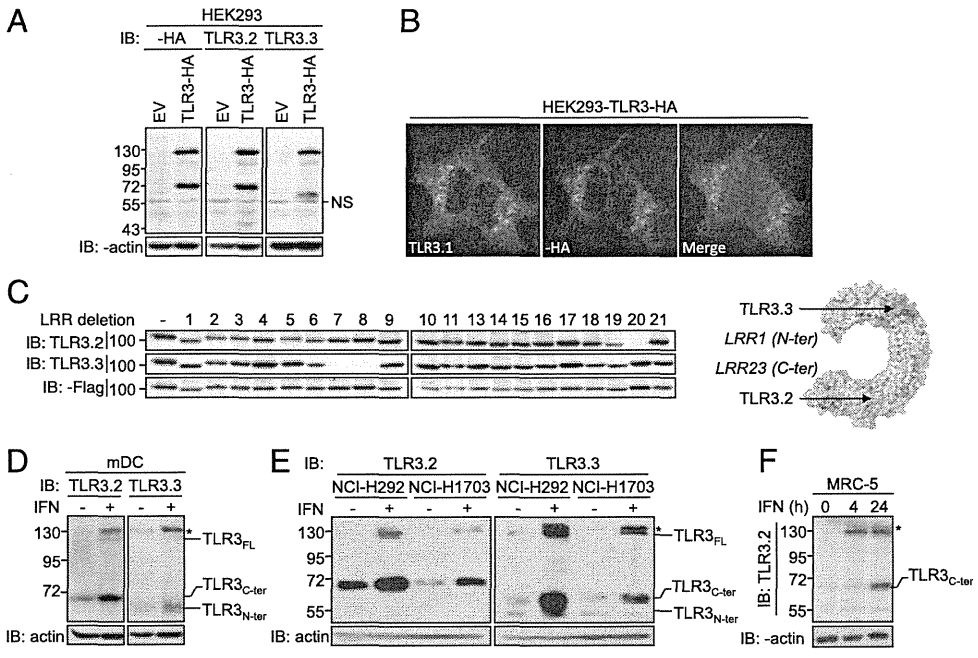

FIGURE 1. Profiling endogenous TLR3 expression. (**A**) Immunoblot analysis of HEK293 cells stably expressing an empty vector (EV) or TLR3-HA; lysates were analyzed with monoclonal anti-HA, TLR3.2, TLR3.3, and anti-actin Abs. (**B**) Immunofluorescence of HEK293 cells stably expressing TLR3-HA; cells were stained with anti-HA or TLR3.1 Abs, followed by DAPI nuclear staining (blue). Original magnification ×63. (**C**) *Left panel*, Epitope mapping of TLR3.2 and TLR3.3 Abs on HEK293 cells stably transfected with TLR3-HA WT (−) or TLR3-HA mutants carrying LRR deletions (1–11 and 13–21, as indicated). Lysates were analyzed with monoclonal TLR3.2, TLR3.3, and anti-Flag Abs, as indicated. *Right panel*, Schematic representation of epitopes recognized by TLR3.2 and TLR3.3 Abs on TLR3 ECD. (**D**) Immunoblot analysis of mDCs treated (+) or not (−) for 18 h with IFN-α (1000 IU/ml); lysates were analyzed with TLR3.2, TLR3.3, and anti-actin Abs. (**E**) Immunoblot analysis of NCI-H292 and NCI-H1703 cells treated (+) or not (−) for 18 h with IFN-α (1000 IU/ml); lysates were analyzed with TLR3.2, TLR3.3, and anti-actin Abs. (**F**) Immunoblot analysis of MRC-5 cells treated (+) or not (−) for the indicated times with IFN-α (1000 IU/ml); lysates were analyzed with TLR3.2 and anti-actin Abs. Values in (A) and (C)–(F) represent molecular mass (kDa). All data are representative of at least three independent experiments. NS, Nonspecific band.

represent the precursors of the latter. In other cell lines, the absolute and relative intensities of the three bands varied depending on the origin of the cells, the Ab used, and the treatment with IFN-α. However, under basal conditions, all cells primarily expressed the 72 and 60 kDa TLR3 forms. Treatment with IFN-α increased the intensity of the three bands and allowed the detection of a higher molecular mass form ~135 kDa in mDCs and in the four cell lines analyzed (asterisk in Fig. 1D–F and Supplemental Fig. 1D). In conclusion, our data suggest that human TLR3 is spontaneously cleaved into a C-terminal fragment ~72 kDa recognized by TLR3.2 and a C-terminal fragment ~60 kDa recognized by TLR3.3, and the relative abundance of cleaved versus uncleaved TLR3 appears to vary with the cell under consideration.

TLR3 ECD cleavage by cathepsins generates two remarkably stable fragments

To further explore the processing of endogenous TLR3 and its functional consequences, we selected the NCI-H292 and NCI-H1703 NSCLC cell lines, which triggered an innate immune response when stimulated with Poly(I:C), as indicated by cytokine secretion (Supplemental Fig. 2A) and by activation of ISRE-dependent luciferase reporter genes (Supplemental Fig. 2B). We ascertained that this response was mediated exclusively by TLR3 by showing its strict dependence on TRIF, the only known adaptor for TLR3 (Supplemental Fig. 2B). We started analyzing the effects of the cathepsin inhibitor Z-FA-fmk on the expression of the different forms of TLR3. Following Z-FA-fmk treatment, the 130 kDa band became more intense with time, whereas the 72 and 60 kDa bands gradually disappeared in both NCI-H292 and NCI-H1703 cells (Fig. 2A, Supplemental Fig. 2C, respectively), as well as in HEK293-TLR3-HA cells (Fig. 2B). These results confirm that cathepsins are necessary for TLR3 cleavage in epithelial cells (22). In NCI-H292 cells, the accumulation of full-length TLR3 was observed as early as 120 min after the addition of Z-FA-fmk (Fig. 2C), whereas in the three cell lines both C-terminal ($TLR3_{C\text{-}ter}$) and N-terminal ($TLR3_{N\text{-}ter}$) TLR3 fragments disappeared with an apparent $t_{1/2}$ >24 h (Fig. 2A, 2B, Supplemental Fig. 2C). Of note, Z-FA-fmk induces a shift of TLR3 full-length ($TLR3_{FL}$) from 130 kDa to 135 kDa ($TLR3_{FL+}$) in both NSCLC cell lines, which is more visible after prolonged gel migration (Fig. 2D). This $TLR3_{FL+}$ could represent the fully glycosylated form of TLR3 leaving the post-Golgi cisternae and not cleaved yet. Published data with regard to the effects of cathepsin inhibitors on TLR3 signaling seem contradictory (8, 9). In this study, we observed that ISRE- and NF-κB–dependent responses to Poly(I:C) were not modified after prolonged treatment with Z-FA-fmk in NCI-H292 cells (Supplemental Fig. 2D), whereas they were significantly, but not completely, suppressed in NCI-H1703 cells (Supplemental Fig. 2E). However, considering the much higher level of TLR3 expression in resting NCI-H292 cells than in NCI-H1703 cells (Fig. 1E), the amounts of $TLR3_{C\text{-}ter}$ detected in NCI-H292 cells after 72 h of treatment with Z-FA-fmk was still comparable to the basal level in NCI-H1703 cells. Therefore, these results suggest that cleaved TLR3 is important for signaling, although uncleaved TLR3 might still transduce some signal. Importantly, Z-FA-fmk treatment blocked TLR3 cleavage and Poly(I:C)-induced cytokine secretion in mDCs (Fig. 2E, 2F) and TR3 signaling in macrophages U937 cells (Fig. 2G, Supplemental Fig. 2F), whereas the response to TNF-α was unaffected. Like with Z-FA-fmk treatment, exposure to the lysosomotropic weak base chloroquine, which prevents cathepsin activity, led to the accumulation of $TLR3_{FL+}$ within 3 h and to the reciprocal disappearance of the two TLR3 fragments in NCI-H292 (Fig. 2H) and NCI-H1703 (Supplemental Fig. 2G) cells after 48 h. The same results were obtained with the specific inhibitor of vacuolar H^+ ATPase Bafilomycin (data not shown). Furthermore, short-term blockade of de novo protein synthesis with cycloheximide confirmed the relative high stability of endogenous $TLR3_{C\text{-}ter}$ (apparent $t_{1/2} >$ 24 h) (Fig. 2I, 2J) compared with $TLR3_{FL}$ (apparent $t_{1/2} < 4$ h). Despite a weaker signal, a half-life similar to $TLR3_{C\text{-}ter}$ was estimated for $TLR3_{N\text{-}ter}$ (Fig. 2H, Supplemental Fig. 2G). Altogether, our data indicate that, in resting cells, TLR3 is actively transcribed and rapidly cleaved by cathepsins upon its transfer in endolysosomes into two highly stable proteolytic fragments, in agreement with a very recent report (26).

TLR3 transits steadily through the Golgi before being cleaved in the endolysosomal compartments

Although TLR3, like other intracellular TLRs, depends on the chaperone protein Unc93b1 for proper trafficking, it is unclear whether its transfer to the endolysosomes occurs constitutively or in response to its ligand. Using TLR3.1 Ab, we observed by immunofluorescence microscopy that TLR3 colocalizes extensively with Lamp1 (a lysosome marker) but not with EEA1 (an early endosome marker) (Fig. 3A, Supplemental Fig. 3) in resting epithelial cells and that the level of colocalization remained unchanged after stimulation with dsRNA (Supplemental Fig. 3). We next addressed the trafficking of TLR3 by analyzing the N-glycosylation status of the protein, which represents ~35% of its total mass (24). After treatments of cell lysates with PNGase, which removes all N-glycans, $TLR3_{FL}$ and $TLR3_{FL+}$ shifted from 130 and 135 kDa, respectively, to 95 kDa (Fig. 3B, 3C), corresponding to the expected molecular mass of nonglycosylated neosynthesized $TLR3_{FL}$ (904 aa). The $TLR3_{C\text{-}ter}$ band shifted from 72 to 50 kDa, indicating that both cleaved and noncleaved TLR3 are glycosylated. Treatment with EndoH, an endoglycosidase that cleaves N-glycans before their further modification in the Golgi apparatus, indicates that noncleaved $TLR3_{FL}$ is EndoH sensitive, whereas $TLR3_{FL+}$ and $TLR3_{C\text{-}ter}$ are partially EndoH resistant. This was similar to the presence of hybrid glycans on TLR9 even after trafficking through the Golgi (27). Cell treatment with tunicamycin, a de novo *N*-glycosylation inhibitor, caused the rapid fading of $TLR3_{FL}$ (apparent $t_{1/2} < 8$ h) and the appearance of a band at ~95 kDa representing neosynthesized nonglycosylated full-length TLR3 (Fig. 3D, 3E). Altogether, our data indicate that $TLR3_{FL}$ corresponds to the small amounts of TLR3 present in the endoplasmic reticulum (ER), which is steadily translocated to the Golgi in resting cells, converted into fully glycosylated $TLR3_{FL+}$, and exported to the endosomes/lysosomes, where it is rapidly cleaved.

The endolysosomal pool of cleaved TLR3 is sufficient for signaling

To determine which forms of endogenous TLR3 are functional, we started using specific siRNA and took advantage of the prolonged stability of cleaved fragments versus $TLR3_{FL}$. We observed that 24 and 48 h after transfection, $TLR3_{FL}$ had completely disappeared, whereas the two cleavage fragments were still abundant (Fig. 4A, Supplemental Fig. 4A). Under these conditions, the Poly(I:C)-induced ISRE-dependent response was not reduced (Fig. 4B), suggesting that the uncleaved $TLR3_{FL}$ does not contribute significantly to downstream signaling, probably because of its weak expression compared with the cleaved fragments from the beginning of the experiment. Indeed, ISRE activation faded away gradually with time as the presence of cleaved TLR3 decreased (Fig. 4A, 4B). Similar results were obtained with a NF-κB–dependent reporter gene (Supplemental Fig. 4B). These data show that cleaved TLR3 can signal in the absence of uncleaved $TLR3_{FL}$ and may even represent the predominant signaling form of the receptor.

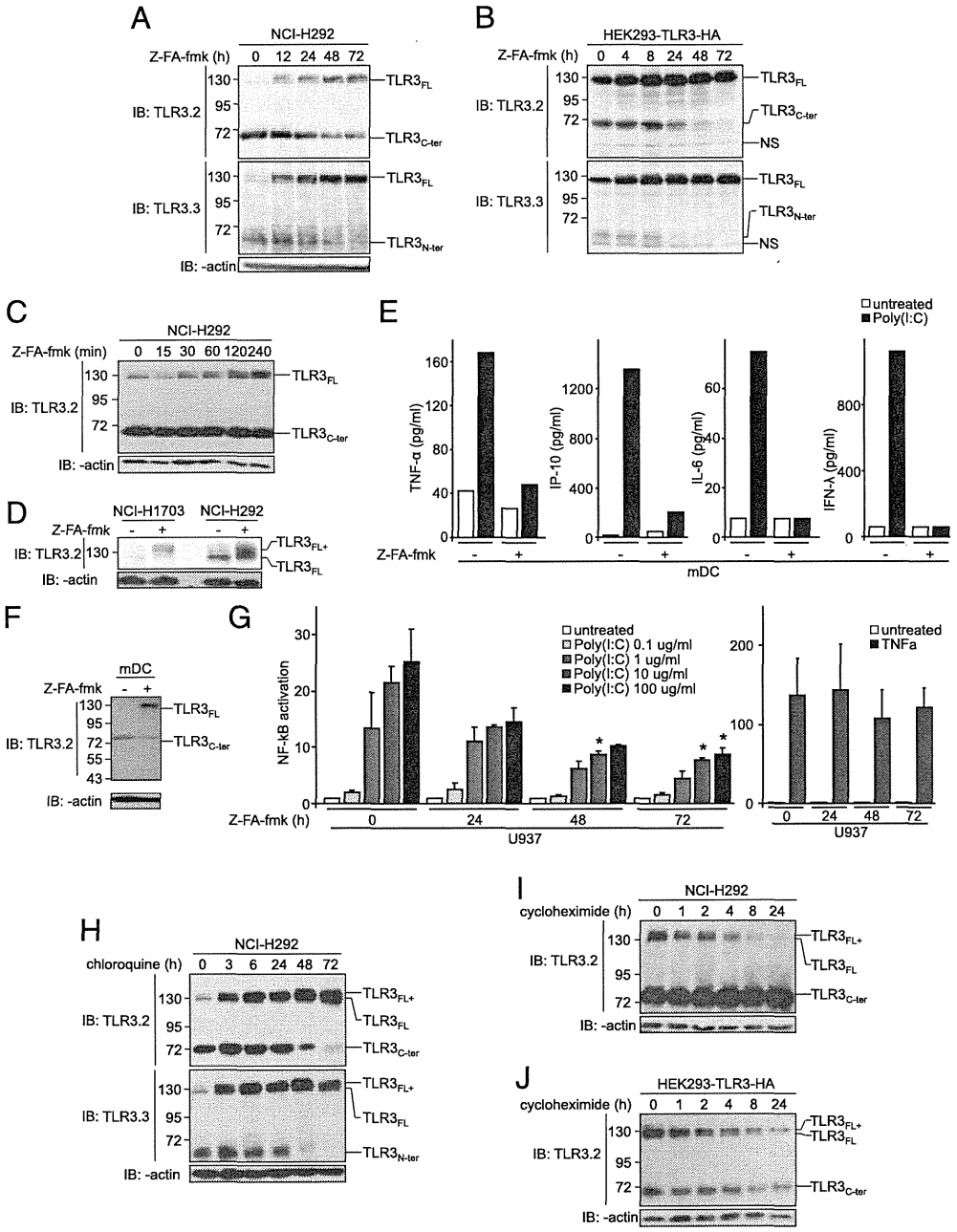

FIGURE 2. Cleavage by cathepsins generates two TLR3 stable fragments. (**A**) Immunoblot analysis of NCI-H292 cells treated for the indicated times with Z-FA-fmk (20 μM) renewed every 24 h. Lysates were analyzed with TLR3.2, TLR3.3, and anti-actin Abs. (**B**) Immunoblot analysis of HEK293-TLR3-HA cells treated for the indicated times with Z-FA-fmk (20 μM) renewed every 24 h. Lysates were analyzed with TLR3.2 and TLR3.3 Abs. (**C**) Immunoblot analysis of NCI-H292 cells treated for the indicated times with Z-FA-fmk (20 μM). Lysates were analyzed with TLR3.2 and anti-actin Abs. (**D**) Immunoblot analysis of NCI-H292 and NCI-H1703 cells treated for 24 h with Z-FA-fmk (20 μM). Lysates were analyzed with TLR3.2 and anti-actin Abs. (**E**) Cytokine production in mDCs that were pretreated for 48 h with Z-FA-fmk and then treated with Poly(I:C) (10 μg/ml) for 24 h. (**F**) Immunoblot analysis of mDCs that were treated or not for 72 h with Z-FA-fmk (20 μM); lysates were analyzed with TLR3.2 and anti-actin Abs. (**G**) NF-κB reporter assay in U937 cells that were pretreated for the indicated times with Z-FA-fmk (20 μM), renewed every 24 h, and then treated with Poly(I:C) at the indicated concentrations (*left panel*) or with TNF-α (50 ng/ml) (*right panel*) for 4 h. (**H**) Immunoblot analysis of NCI-H292 cells treated for the indicated times with chloroquine (1 μg/ml). Lysates were analyzed with TLR3.2, TLR3.3, and anti-actin Abs. (**I**) Immunoblot analysis of NCI-H292 cells treated for the indicated times with cycloheximide (1.5 μg/ml). Lysates were analyzed with TLR3.2 and anti-actin Abs. (**J**) Immunoblot analysis of HEK293-TLR3-HA cells treated for the indicated times with cycloheximide (1.5 μg/ml). Lysates were analyzed with TLR3.2 and anti-actin Abs. Values represent molecular mass (kDa). Data are mean (G) or representative (A–F, H–J) of at least three independent experiments. $*p < 0.05$, untreated cells versus Z-FA-fmk–treated cells.

The N- and C-terminal fragments of TLR3 ECD are needed for efficient signaling

To definitely establish the functionality of uncleaved versus cleaved TLR3, we expressed three mutants of TLR3 in HEK293 cells. Given the apparent molecular mass of deglycosylated $TLR3_{C\text{-}ter}$ and $TLR3_{FL}$ (50 and 95 kDa, respectively; Fig. 3B, 3C), the highly conserved insertion within LRR12, which protrudes on the glycosylation-free side of LRR12 (residues 335–342) (28–31), was a likely site for proteolysis. Thus, the first mutant lacked the entire LRR12 insertion (TLR3-Ins12-HA), whereas the two others represented the C-terminal fragment starting just at the end of the LRR12 insertion (aa 346: TLR3-$Cter_{346}$-HA), as established and

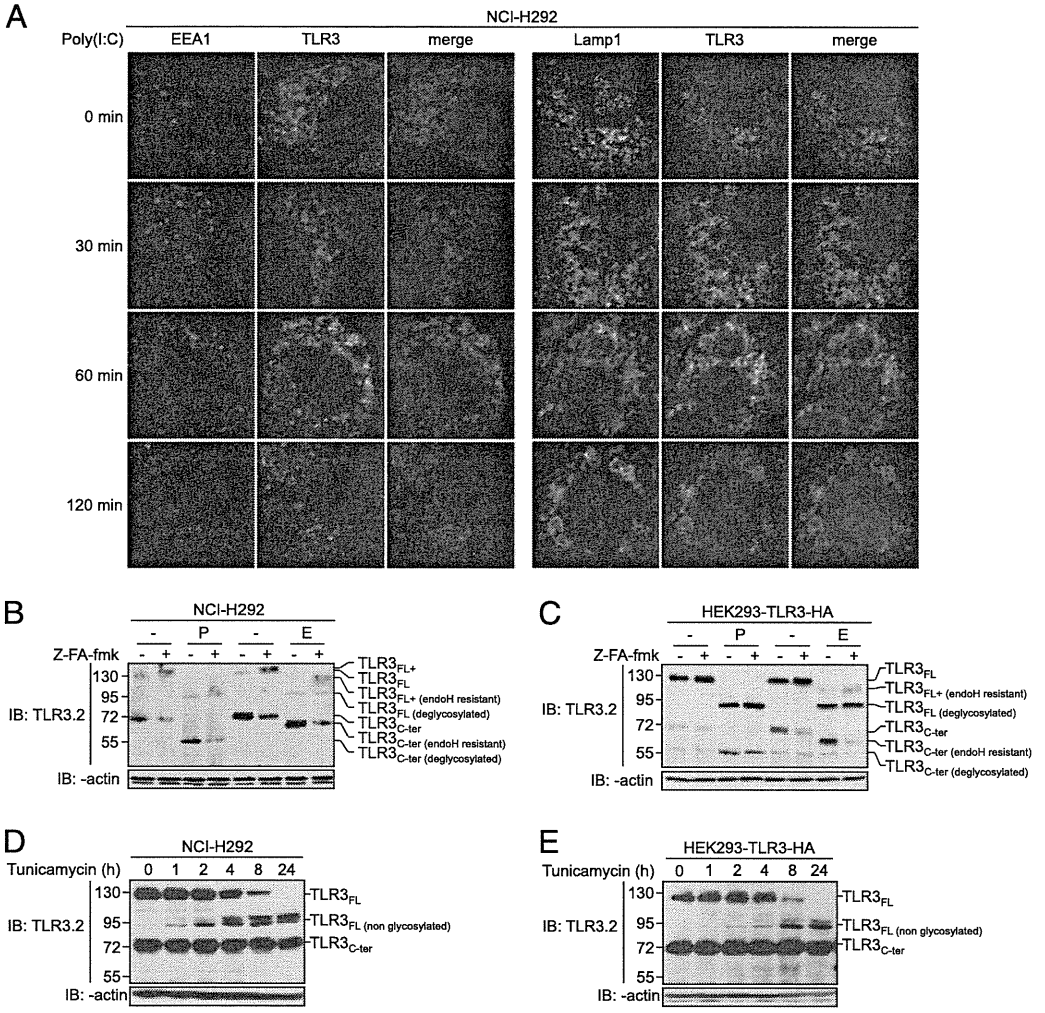

FIGURE 3. TLR3 transits through the Golgi before being cleaved in the endolysosomal compartments. (**A**) Immunofluorescence of NCI-H292 cells treated for the indicated times with Poly(I:C) (10 μg/ml) and then stained with EEA1 or Lamp1, and TLR3.1 Abs, followed by DAPI nuclear staining (blue). Original magnification ×63. (**B**) Immunoblot analysis of NCI-H292 cells that were treated or not with Z-FA-fmk (20 μM) for 24 h. Lysates were left untreated (−) or were treated (+) with PNGase (P) or EndoH (E) and then analyzed with TLR3.2 and anti-actin Abs. (**C**) Immunoblot analysis of HEK293-TLR3-HA cells that were treated or not with Z-FA-fmk (20 μM) for 24 h. Lysates were left untreated (−) or were treated (+) with PNGase (P) or EndoH (E) and then analyzed with TLR3.2 and anti-actin Abs. (**D**) Immunoblot analysis of NCI-H292 cells that were treated for the indicated times with tunicamycin (1 μg/ml). Lysates were analyzed with TLR3.2 and anti-actin Abs. (**E**) Immunoblot analysis of HEK293-TLR3-HA cells that were treated for the indicated times with tunicamycin (1 μg/ml). Lysates were analyzed with TLR3.2 and anti-actin Abs. Values in (B)–(D) represent molecular mass (kDa). Data are representative of at least three independent experiments.

characterized by Garcia-Cattaneo et. al (22), or at the beginning of LRR13 (aa 356: TLR3-Cter$_{356}$-HA) (Fig. 5A). Immunoblots confirmed that all three constructs were expressed at comparable levels in HEK-293T–transfected cells (Fig. 5B), with TLR3-Ins12-HA expressed as a single 130-kDa band, confirming that the LRR12 insertion contains the cleavage site and that TLR3-Ins12-HA is a noncleavable form of the receptor. As expected, lysates from TLR3-Cter$_{356}$-HA– or TLR3-Cter$_{346}$-HA–transfected cells contained a single form ~72 kDa, whose size is consistent with the predicted length of each construct (Fig. 5B). We also observed that treatment with Poly(I:C) did not modify the processing of TLR3 and, particularly, did not induce the cleavage of TLR3-Ins12-HA (Fig. 5B).

When expressed in HEK293 cells, the noncleavable form of the receptor showed the capacity to activate ISRE- and NF-κB–dependent transcription in response to 10 μg/ml of Poly(I:C) (Fig. 5C)

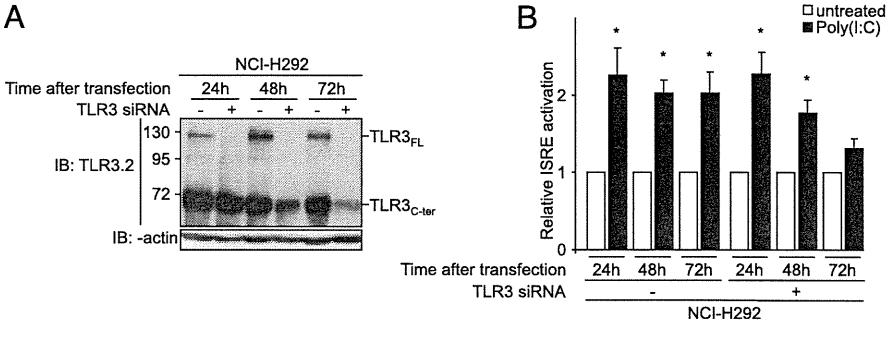

FIGURE 4. Endogenous cleaved TLR3 is sufficient to fully signal. (**A**) Immunoblot analysis of NCI-H292 cells at the indicated times after nonsilencing (−) or TLR3 (+) siRNA transfections (25 μM). Lysates were analyzed with TLR3.2 and anti-actin Abs. (**B**) ISRE reporter assay in NCI-H292 cells at the indicated times after nonsilencing (−) or TLR3 (+) siRNA transfections (25 μM) and treatment without or with Poly(I:C) (10 μg/ml) for 4 h. Data are representative (A) or the mean (B) of three independent experiments. Error bars represent SEM. *$p < 0.05$, untreated cells versus Poly(I:C)-treated cells.

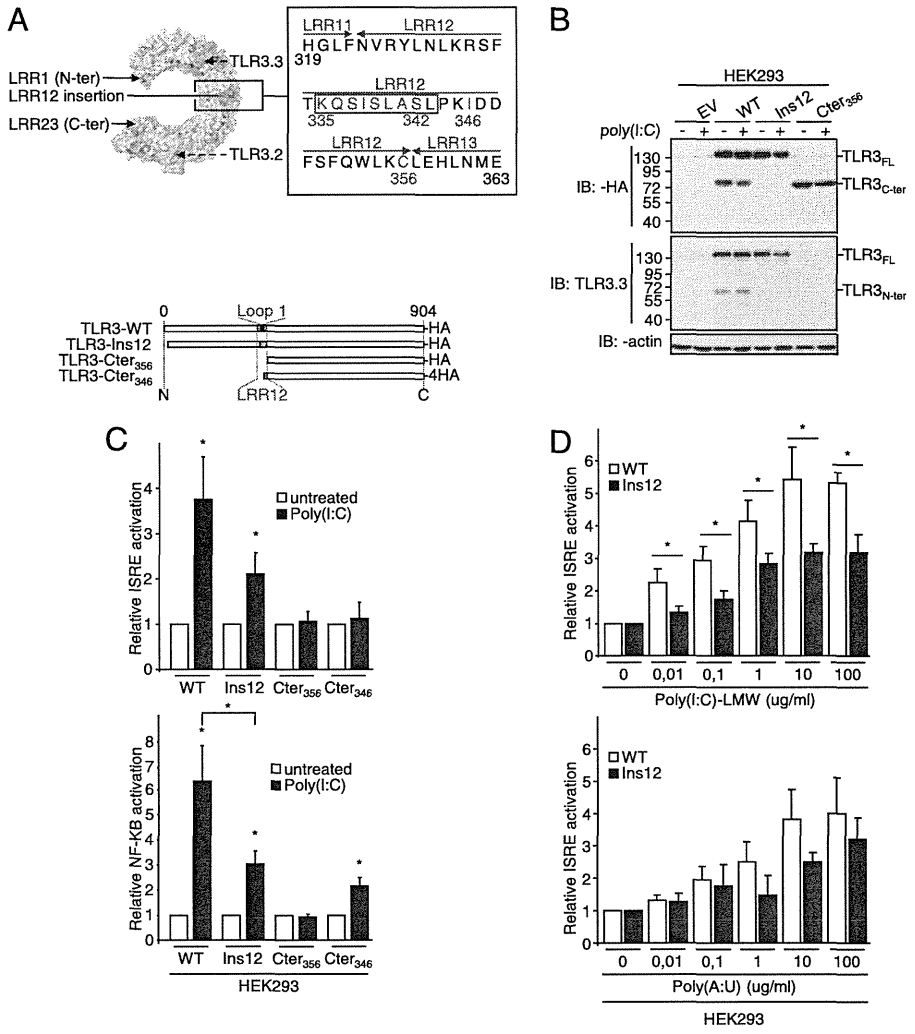

FIGURE 5. Noncleaved TLR3 can signal but the isolated C-terminal TLR3 fragment cannot. (**A**) *Upper panel*, Model of the putative location of the cleavage on LRR12 and TLR3 sequence with starting points of TLR3-Cter$_{356}$ and TLR3-Cter$_{346}$ mutants and deleted sequence (aa 335–342) of TLR3-Ins12 (in red). Blue framework: LRR12 loop1. *Lower panel*, Schematic representation of TLR3 mutants. (**B**) Immunoblot analysis of HEK293 cells transfected with empty vector (EV), TLR3-WT-HA (WT), TLR3-Ins12-HA (Ins12), or TLR3-Cter$_{356}$-HA (Cter$_{356}$) and then treated without (−) or with (+) Poly(I:C) (10 μg/ml) for 4 h. Lysates were analyzed with anti-HA, TLR3.3, and anti-actin Abs. Values represent molecular mass (kDa). (**C**) ISRE (*upper panel*) and NF-KB (*lower panel*) reporter assay in HEK293 cells transfected with TLR3-WT-HA, TLR3-Ins12-HA, TLR3-Cter$_{356}$-HA (Cter$_{356}$), or TLR3-Cter$_{346}$-HA (Cter$_{346}$), and then treated without (white) or with (black) Poly(I:C) (10 μg/ml) for 6 h. (**E**) ISRE reporter assay in HEK293 cells transfected with TLR3-WT-HA or TLR3-Ins12-HA and then treated with the indicated concentrations of Poly(I:C)-LMW or Poly(A:U) for 6 h. Data are representative (B) or the mean (C, D) of at least three independent experiments. Error bars (C, D) represent SEM. *$p < 0.05$, untreated versus Poly(I:C)-treated cells or response of TLR3-WT versus mutant TLR3.

but with significantly reduced efficiency for NF-κB compared with WT TLR3. In contrast, TLR3-Cter$_{356}$-HA was unable to activate either pathway, and TLR3-Cter$_{346}$-HA triggered a weak NF-κB response but no ISRE-dependent response. We next compared the levels of ISRE-dependent transcription in response to increasing concentrations of either LMW Poly(I:C) or Poly(A:U). The dose responses showed that HEK293 cells transfected with WT TLR3 were also significantly more sensitive to LMW Poly(I:C) but not to Poly(A:U) (Fig. 5D). Notably, both C-terminal fragments of the receptor were completely unresponsive to all doses of these two ligands (data not shown). Taken together, these results show that, in agreement with previous reports, uncleaved TLR3 can generate a response to dsRNA (30), whereas the isolated C-terminal fragment triggers only a weak signal (26).

The N- and C-terminal fragments of TLR3 remain associated after cleavage

Because cleaved TLR3 was able to signal in the total absence of TLR3$_{FL}$ (Fig. 4A, 4B, Supplemental Fig. 4A, 4B), whereas isolated TLR3$_{C\text{-}ter}$ was almost ineffective (Fig. 5C), we wondered whether the two fragments of TLR3 could remain associated after proteolytic cleavage. Therefore, we compared the profiles of TLR3 on Western blot performed with lysates prepared in nondenaturing (protein lysate neither reduced nor heated) versus denaturing conditions (Fig. 6A–D, Supplemental Fig. 4C). In nondenaturing conditions, we detected the 130 kDa band, whereas bands corresponding to the proteolytic fragments were barely detectable in epithelial NCI-H292 cells (Fig. 6A, Supplemental Fig. 4C), in mDCs (Fig. 6B), as well as in HEK293-TLR3-HA cells (Fig. 6C, 6D). We ensured that nondenaturing conditions did not prevent the migration of TLR3 fragments, because the constructs corresponding to the cleaved TLR3$_{C\text{-}ter}$ fragment (Cter$_{356}$ and Cter$_{346}$) migrated at expected molecular mass (~72 kDa; Fig. 6D). In contrast, when the same lysates were analyzed in denaturing conditions, TLR3$_{C\text{-}ter}$ and TLR3$_{N\text{-}ter}$ became clearly visible (Fig. 6A–D, Supplemental Fig. 4C), thereby revealing the presence of both uncleaved and cleaved/associated TLR3 in cells. Similarly, when nondenatured lysates were immunoblotted after running on a native gel, the same high molecular band was observed, with HEK293 cells expressing either WT or noncleavable TLR3 and with epithelial cells expressing endogenous TLR3 (Supplemental Fig. 4D). In contrast, the TLR3$_{C\text{-}ter}$ mutant migrated on the same gel at a much lower molecular mass. Moreover, nondenaturing conditions showed that Poly(I:C) treatment did not dissociate TLR3$_{C\text{-}ter}$ and TLR3$_{N\text{-}ter}$ (Fig. 6A–C, Supplemental Fig. 4C). To definitely confirm the association of the two cleaved fragments, we performed immunoprecipitation with C-terminal–specific TLR3.2 and N-terminal–specific TLR3.3 Abs and analyzed the precipitates by immunoblot with the two Abs. In all cases, TLR3$_{N\text{-}ter}$ and TLR3$_{C\text{-}ter}$ coimmunoprecipitated both in NCI-H292 cells (Fig. 6E) and HEK293-TLR3-HA cells (Fig. 6F). Lastly, reprecipitation after denaturation of the immunoprecipitates ob-

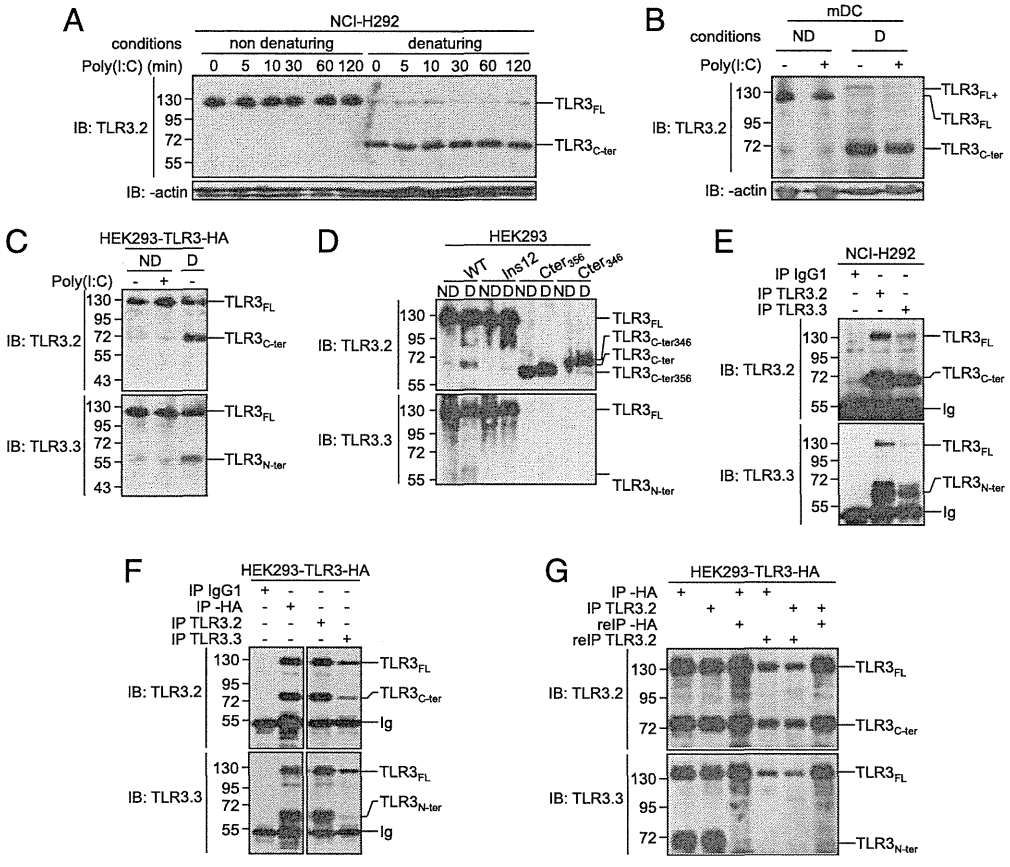

FIGURE 6. The N- and C-terminal fragments of endogenous TLR3 fragments remain associated after cleavage. (**A**) Immunoblot analysis of NCI-H292 cells treated with Poly(I:C) (10 μg/ml) for the indicated times. Lysates were denatured (D) or not (ND) and then analyzed with TLR3.2 and anti-actin Abs. (**B**) Immunoblot analysis of mDCs treated (+) or not (−) with Poly(I:C) (10 μg/ml) for the indicated times. Lysates were denatured (D) or not (ND) and then analyzed with TLR3.2 and anti-actin Abs. (**C**) Immunoblot analysis of HEK293-TLR3-HA cells treated (+) or not (−) with Poly(I:C) (10 μg/ml) for 2 h. Lysates were denatured (D) or not (ND) and then analyzed with TLR3.2 and TLR3.3 Abs. (**D**) Immunoblot analysis of HEK293 cells transfected with TLR3-WT-HA (WT), TLR3-Ins12-HA (Ins12), TLR3-Cter$_{356}$-HA (Cter$_{356}$), or TLR3-Cter$_{346}$-HA (Cter$_{346}$). Lysates were denatured (D) or not (ND) and then analyzed with TLR3.2 and TLR3.3 Abs. (**E**) Immunoblot analysis of NCI-H292 cells. Lysates were immunoprecipitated with IgG1, TLR3.2, or TLR3.3 Abs and analyzed with TLR3.2 and TLR3.3 Abs. (**F**) Immunoblot analysis of HEK293-TLR3-HA cells. Lysates were immunoprecipitated with IgG1, anti-HA, TLR3.2, or TLR3.3 Abs and analyzed with TLR3.2 and TLR3.3 Abs. (**G**) Immunoblot analysis of HEK293-TLR3-HA cells. Lysates were immunoprecipitated with anti-HA or TLR3.2 Abs and then precipitates were reimmunoprecipitated with anti-HA or TLR3.2 Abs and analyzed with TLR3.2 and TLR3.3 Abs. Values represent molecular mass (kDa). Data are representative of at least three independent experiments.

tained with a C-terminal–specific Ab (either TLR3.2 or anti-HA) led to the loss of the N-terminal fragment of TLR3, confirming that the association of the two fragments was through a noncovalent bond (Fig. 6G). Taken together, our data show that the two fragments of TLR3 remain associated after cleavage and that ligand binding does not disrupt this association (Fig. 7). Therefore, the cleaved/associated TLR3 represents the relevant endogenous TLR3 responsible for the majority of immunological functions.

Discussion

Remarkable progress has been made recently in our understanding of the biology of nucleic acid–sensing TLR3, TLR7, and TLR9. Notably, various data now suggest a model in which exogenous nucleotides can be recognized with high sensitivity, whereas self-nucleotide–induced signaling and autoimmunity are prevented (3). Discrimination between nonself- and self-nucleotides appears to be facilitated by several levels of regulation. Recently, cleavage of TLR9 in endolysosomes was shown to be required for generating the C-terminal fragment of the receptor that binds dsDNA with high affinity and signals. Published data indicated that this mechanism might also apply to TLR3 and TLR7 (9, 22). However, our data allow us to propose an alternative model for TLR3 biology (Fig. 7), which reconciles two requisites: the need to restrict dsRNA recognition in endolysosomes (and therefore to expose the receptor to a proteolytic environment) to prevent autoreactivity, as described for other endosomal TLRs, and the requirement of the two ligand binding sites present on the ECD of TLR3—the first near the N terminus and the second close to the transmembrane region—to recognize dsRNA with high avidity. Several aspects of the trafficking and processing of TLR3 diverge from what has been described for other lysosomal TLRs (8, 10).

Building on previous observations, and supported by data that were published after the submission of our manuscript (26), our results allow improvement of our model of TLR3 biology. In contrast to TLR9, which was reported to reside principally in the ER in resting cells (32) and to reach the acidic compartments after stimulation by double-stranded DNA (5–7, 33), TLR3 is continuously exported to the Golgi and accumulates in the endolysosomal compartments where it undergoes a single cleavage by cathepsins, most likely within the short (9 aa) LRR12 external loop; however, the exact cleavage site remains unknown. In contrast, asparagine endopeptidase first cleaves the long (30 aa) LRR14–15 flexible loop of TLR9 that is secondarily trimmed by cathepsins (8–10, 34, 35). Strong conservation of the LRR12 ex-

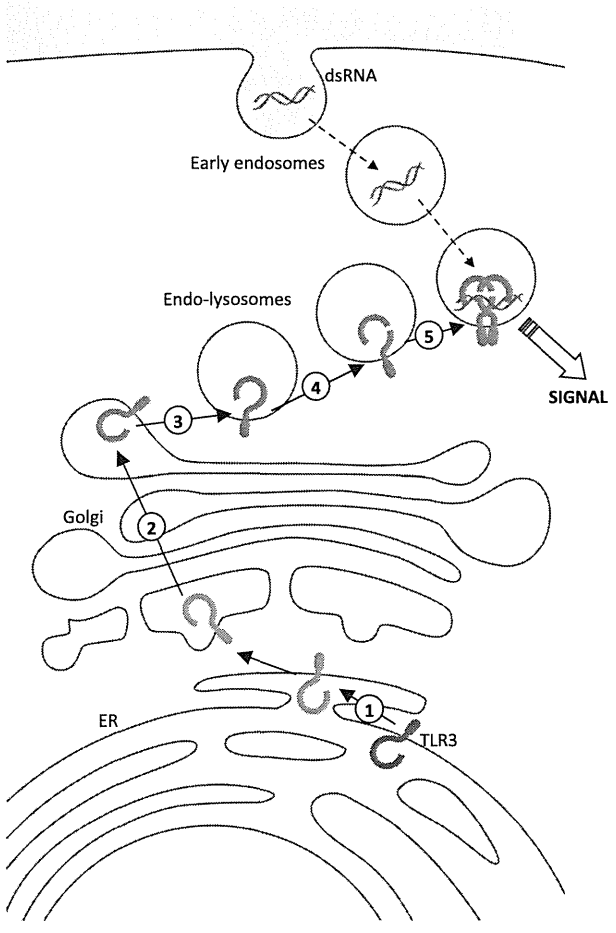

FIGURE 7. Proposed model of TLR3 processing. (**1**) TLR3 is neosynthesized and *N*-glycosylated in the ER. (**2**) Then, it crosses the Golgi apparatus where it is fully glycosylated to become EndoH resistant. TLR3 exits the Golgi to enter the endosome membrane (**3**) where it is cleaved by cathepsins (**4**). The two proteolytic fragments remain associated to fully signal (**5**).

ternal loop (residues 335–343) during mammals' evolution (30) suggests that cleavage is an important step in the biology of TLR3. Remarkably, our data confirm that the two proteolytic fragments of the ECD of TLR3 have prolonged half-lives (26) and demonstrate that they remain associated, suggesting that the noncovalent interactions between the adjacent LRRs known to stabilize the ECD of TLRs (36) have been preserved. Furthermore, the absence of detectable amounts of Golgi-modified $TLR3_{FL+}$ in resting immune and nonimmune cells (Figs. 1A, 1D–F, 3B, 3C) indicates that cleaved/associated TLR3 is the almost exclusive form of the receptor present in endolysosomes, where the encounter with exogenous dsRNA is known to occur (37). The lack of appropriate ligand prevented us from visualizing directly TLR3 bound to dsRNA. However, the physical association of TRIF with $TLR3_{C\text{-}ter}$, but not $TLR3_{FL}$, after activation with Poly(I:C) in NCI-H292 cells (38), combined with the absence of free $TLR3_{C\text{-}ter}$ in those cells, indicates that cleaved/associated TLR3 is the main form of the receptor recognizing Poly(I:C). The single cleavage, without further trimming, may explain why the two long-lived fragments of TLR3 remain associated to bind dsRNA. In contrast, although it was proposed that some TLR9 fragments could remain associated (8, 39), the C-terminal fragment of the receptor is viewed as the major form of the functional receptor, binding agonist CpG oligodesoxynucleotides with high affinity and being able to efficiently recruit the adaptor protein MyD88 (8, 10).

The streamlined transfer to endolysosomes, followed by rapid cleavage, explains why endogenous TLR3 fragments were abundant in resting cells of every type analyzed, whereas $TLR3_{FL}$ was difficult to detect. In contrast, comparable amounts of $TLR3_{FL}$ and TLR3 fragments were observed in HEK293 cells, suggesting an imbalance between the high expression of exogenous TLR3 and the availability of the chaperone protein Unc93b1 in those cells (26). Indeed, exogenous TLR3 was abundant in the ER, whereas endogenous TLR3 was found mostly in the endolysosomes. Moreover, the half-lives of the fragments from transfected TLR3 were shorter compared with endogenous TLR3 (compare Fig. 2B with Fig. 2A). These differences should be kept in mind when studying the biology of endosomal TLRs in HEK293 cells.

TLR3 cleavage could increase or decrease the sensitivity of the receptor and/or modify its specificity for different ligands. Our functional studies reveal that, in TLR3-transfected HEK293 cells, the cleavage increased the sensitivity to HMW and LMW Poly(I:C). The increased sensitivity of cleaved/associated TLR3 remains perplexing. Thus, cleavage could somehow increase the affinity of the ECD for its ligands or ease the conformational change that may occur in the presence of dsRNA (39) and that may facilitate the recruitment of TRIF. In agreement with Qi et al. (26), we observed that $TLR3_{C\text{-}ter}$ by itself was consistently unable to trigger a strong response to dsRNA. A difference in timing (6 versus 18 h) might explain, in part, the variance between those results and recently published data that showed an equal response to Poly(I:C) with either TLR3-WT or $TLR3_{C\text{-}ter}$ (22). Whatsoever the residual activity of $TLR3_{C\text{-}ter}$, its physiological importance is uncertain, because cleaved/associated TLR3 appears to be the predominant form of the endogenous receptor present in the endolysosomes where recognition of dsRNA takes place.

The central role of cleaved/associated TLR3 highlights the importance for dsRNA binding affinity and sensitive signaling of two distinct ligand-binding sites, each present on one proteolytic fragment. Moreover, the increased sensitivity to Poly(I:C) and the remarkable stability of this form of the receptor allows the reconciliation of some apparently discordant results from the literature. Indeed, one group reported the absence of inhibition of TNF production by RAW macrophages treated for 12 h with cathepsin inhibitors and then for 2 h with 100 μg/ml of Poly(I:C) (8), whereas another group showed a strong suppression of TNF production by the same cells in response to 1 μg/ml of Poly(I:C) (9). These different outcomes may be due to differences in the concentration of ligand used, with high concentrations of dsRNA being able to activate the less efficient $TLR3_{FL}$ in these cells. In addition, our data show that 12 h of Z-FA-fmk pretreatment is not sufficient to suppress the expression of TLR3 fragments in NSCLC cells, suggesting that the lack of inhibition by Z-FA-fmk of cells activated with moderate concentrations of Poly(I:C) could have resulted from the persistence of some cleaved/associated TLR3 at the time of stimulation.

In conclusion, TLR3 provides the first example, to our knowledge, of endosomal receptor maturation by cleavage followed by conversion into a functional cleaved/associated form of the protein. Considering that cleavage of WT-TLR3 is necessary for signaling, cleaved/associated TLR3 is the principal (and possibly exclusive) signaling receptor, and noncleavable TLR3 is able to signal, an intriguing conclusion of the present work is that the licensing consequence of TLR3 cleavage for signaling is not the separation of the two fragments. Further studies are required to fully evaluate the structural and functional consequences of TLR3 processing in vitro and in vivo, as well as to determine to what extent some aspects of TLR3 biology might apply to the other endolysosomal TLRs.

Acknowledgments

We thank Olivier Micheau (Bourgogne University, Dijon, France) for critical reading of the manuscript, Philippe Benaroch for reviewing the results and for the plasmid gift, and Sebastian Amigorena for discussions (both at Curie Institute, Paris, France).

Disclosures

The authors have no financial conflicts of interest.

References

1. Kawai, T., and S. Akira. 2011. Toll-like receptors and their crosstalk with other innate receptors in infection and immunity. *Immunity* 34: 637–650.
2. Gay, N. J., and M. Gangloff. 2007. Structure and function of Toll receptors and their ligands. *Annu. Rev. Biochem.* 76: 141–165.
3. Barton, G. M., and J. C. Kagan. 2009. A cell biological view of Toll-like receptor function: regulation through compartmentalization. *Nat. Rev. Immunol.* 9: 535–542.
4. Limmon, G. V., M. Arredouani, K. L. McCann, R. A. Corn Minor, L. Kobzik, and F. Imani. 2008. Scavenger receptor class-A is a novel cell surface receptor for double-stranded RNA. *FASEB J.* 22: 159–167.
5. Barton, G. M., J. C. Kagan, and R. Medzhitov. 2006. Intracellular localization of Toll-like receptor 9 prevents recognition of self DNA but facilitates access to viral DNA. *Nat. Immunol.* 7: 49–56.
6. Tabeta, K., K. Hoebe, E. M. Janssen, X. Du, P. Georgel, K. Crozat, S. Mudd, N. Mann, S. Sovath, J. Goode, et al. 2006. The Unc93b1 mutation 3d disrupts exogenous antigen presentation and signaling via Toll-like receptors 3, 7 and 9. *Nat. Immunol.* 7: 156–164.
7. Kim, Y.-M., M. M. Brinkmann, M.-E. Paquet, and H. L. Ploegh. 2008. UNC93B1 delivers nucleotide-sensing toll-like receptors to endolysosomes. *Nature* 452: 234–238.
8. Park, B., M. M. Brinkmann, E. Spooner, C. C. Lee, Y.-M. Kim, and H. L. Ploegh. 2008. Proteolytic cleavage in an endolysosomal compartment is required for activation of Toll-like receptor 9. *Nat. Immunol.* 9: 1407–1414.
9. Ewald, S. E., A. Engel, J. Lee, M. Wang, M. Bogyo, and G. M. Barton. 2011. Nucleic acid recognition by Toll-like receptors is coupled to stepwise processing by cathepsins and asparagine endopeptidase. *J. Exp. Med.* 208: 643–651.
10. Ewald, S. E., B. L. Lee, L. Lau, K. E. Wickliffe, G.-P. Shi, H. A. Chapman, and G. M. Barton. 2008. The ectodomain of Toll-like receptor 9 is cleaved to generate a functional receptor. *Nature* 456: 658–662.
11. Alexopoulou, L., A. C. Holt, R. Medzhitov, and R. A. Flavell. 2001. Recognition of double-stranded RNA and activation of NF-kappaB by Toll-like receptor 3. *Nature* 413: 732–738.
12. Casrouge, A., S.-Y. Zhang, C. Eidenschenk, E. Jouanguy, A. Puel, K. Yang, A. Alcais, C. Picard, N. Mahfoufi, N. Nicolas, et al. 2006. Herpes simplex virus encephalitis in human UNC-93B deficiency. *Science* 314: 308–312.
13. Zhang, S.-Y., E. Jouanguy, S. Ugolini, A. Smahi, G. Elain, P. Romero, D. Segal, V. Sancho-Shimizu, L. Lorenzo, A. Puel, et al. 2007. TLR3 deficiency in patients with herpes simplex encephalitis. *Science* 317: 1522–1527.
14. Guo, Y., M. Audry, M. Ciancanelli, L. Alsina, J. Azevedo, M. Herman, E. Anguiano, V. Sancho-Shimizu, L. Lorenzo, E. Pauwels, et al. 2011. Herpes simplex virus encephalitis in a patient with complete TLR3 deficiency: TLR3 is otherwise redundant in protective immunity. *J. Exp. Med.* 208: 2083–2098.
15. Matsumoto, M., H. Oshiumi, and T. Seya. 2011. Antiviral responses induced by the TLR3 pathway. *Rev. Med. Virol.* 21: 67–77.
16. Karikó, K., H. Ni, J. Capodici, M. Lamphier, and D. Weissman. 2004. mRNA is an endogenous ligand for Toll-like receptor 3. *J. Biol. Chem.* 279: 12542–12550.
17. Wang, Y., L. Liu, D. R. Davies, and D. M. Segal. 2010. Dimerization of Toll-like receptor 3 (TLR3) is required for ligand binding. *J. Biol. Chem.* 285: 36836–36841.
18. Bell, J. K., J. Askins, P. R. Hall, D. R. Davies, and D. M. Segal. 2006. The dsRNA binding site of human Toll-like receptor 3. *Proc. Natl. Acad. Sci. USA* 103: 8792–8797.
19. Liu, L., I. Botos, Y. Wang, J. N. Leonard, J. Shiloach, D. M. Segal, and D. R. Davies. 2008. Structural basis of toll-like receptor 3 signaling with double-stranded RNA. *Science* 320: 379–381.
20. Fukuda, K., T. Tsujita, M. Matsumoto, T. Seya, H. Sakiyama, F. Nishikawa, S. Nishikawa, and T. Hasegawa. 2006. Analysis of the interaction between human TLR3 ectodomain and nucleic acids. *Nucleic Acids Symp. Ser. (Oxf)* 50: 249–250.
21. Watanabe, T., T. Tokisue, T. Tsujita, M. Matsumoto, T. Seya, S. Nishikawa, T. Hasegawa, and K. Fukuda. 2007. N-terminal binding site in the human toll-like receptor 3 ectodomain. *Nucleic Acids Symp. Ser. (Oxf)* 51: 405–406.
22. Garcia-Cattaneo, A., F. X. Gobert, M. Müller, F. Toscano, M. Flores, A. Lescure, E. Del Nery, and P. Benaroch. 2012. Cleavage of Toll-like receptor 3 by cathepsins B and H is essential for signaling. *Proc. Natl. Acad. Sci. USA* 109: 9053–9058.
23. Takada, E., S. Okahira, M. Sasai, K. Funami, T. Seya, and M. Matsumoto. 2007. C-terminal LRRs of human Toll-like receptor 3 control receptor dimerization and signal transmission. *Mol. Immunol.* 44: 3633–3640.
24. Sun, J., K. E. Duffy, C. T. Ranjith-Kumar, J. Xiong, R. J. Lamb, J. Santos, H. Masarapu, M. Cunningham, A. Holzenburg, R. T. Sarisky, et al. 2006. Structural and functional analyses of the human Toll-like receptor 3. Role of glycosylation. *J. Biol. Chem.* 281: 11144–11151.
25. Kaiser, W. J., J. L. Kaufman, and M. K. Offermann. 2004. IFN-α sensitizes human umbilical vein endothelial cells to apoptosis induced by double-stranded RNA. *J. Immunol.* 172: 1699–1710.
26. Qi, R., D. Singh, and C. C. Kao. 2012. Proteolytic processing regulates Toll-like receptor 3 stability and endosomal localization. *J. Biol. Chem.* 287: 32617–32629.
27. Chockalingam, A., J. C. Brooks, J. L. Cameron, L. K. Blum, and C. A. Leifer. 2009. TLR9 traffics through the Golgi complex to localize to endolysosomes and respond to CpG DNA. *Immunol. Cell Biol.* 87: 209–217.
28. Bell, J. K., I. Botos, P. R. Hall, J. Askins, J. Shiloach, D. M. Segal, and D. R. Davies. 2005. The molecular structure of the Toll-like receptor 3 ligand-binding domain. *Proc. Natl. Acad. Sci. USA* 102: 10976–10980.
29. Choe, J., M. S. Kelker, and I. A. Wilson. 2005. Crystal structure of human toll-like receptor 3 (TLR3) ectodomain. *Science* 309: 581–585.
30. Ranjith-Kumar, C. T., W. Miller, J. Xiong, W. K. Russell, R. Lamb, J. Santos, K. E. Duffy, L. Cleveland, M. Park, K. Bhardwaj, et al. 2007. Biochemical and functional analyses of the human Toll-like receptor 3 ectodomain. *J. Biol. Chem.* 282: 7668–7678.
31. Botos, I., L. Liu, Y. Wang, D. M. Segal, and D. R. Davies. 2009. The toll-like receptor 3:dsRNA signaling complex. *Biochim. Biophys. Acta* 1789: 667–674.
32. Leifer, C. A., M. N. Kennedy, A. Mazzoni, C. Lee, M. J. Kruhlak, and D. M. Segal. 2004. TLR9 is localized in the endoplasmic reticulum prior to stimulation. *J. Immunol.* 173: 1179–1183.
33. Latz, E., A. Schoenemeyer, A. Visintin, K. A. Fitzgerald, B. G. Monks, C. F. Knetter, E. Lien, N. J. Nilsen, T. Espevik, and D. T. Golenbock. 2004. TLR9 signals after translocating from the ER to CpG DNA in the lysosome. *Nat. Immunol.* 5: 190–198.
34. Kasperkovitz, P. V., M. L. Cardenas, and J. M. Vyas. 2010. TLR9 is actively recruited to *Aspergillus fumigatus* phagosomes and requires the N-terminal proteolytic cleavage domain for proper intracellular trafficking. *J. Immunol.* 185: 7614–7622.
35. Sepulveda, F. E., S. Maschalidi, R. Colisson, L. Heslop, C. Ghirelli, E. Sakka, A.-M. Lennon-Duménil, S. Amigorena, L. Cabanie, and B. Manoury. 2009. Critical role for asparagine endopeptidase in endocytic Toll-like receptor signaling in dendritic cells. *Immunity* 31: 737–748.
36. Manavalan, B., S. Basith, and S. Choi. 2011. Similar structures but different roles – an updated perspective on TLR structures. *Front. Physiol.* 2: 41.
37. de Bouteiller, O., E. Merck, U. A. Hasan, S. Hubac, B. Benguigui, G. Trinchieri, E. E. Bates, and C. Caux. 2005. Recognition of double-stranded RNA by human toll-like receptor 3 and downstream receptor signaling requires multimerization and an acidic pH. *J. Biol. Chem.* 280: 38133–38145.
38. Estornes, Y., F. Toscano, F. Virard, G. Jacquemin, A. Pierrot, B. Vanbervliet, M. Bonnin, N. Lalaoui, P. Mercier-Gouy, Y. Pachéco, et al. 2012. dsRNA induces apoptosis through an atypical death complex associating TLR3 to caspase-8. *Cell Death Differ.* 19: 1482–1494.
39. Li, Y., I. C. Berke, and Y. Modis. 2012. DNA binding to proteolytically activated TLR9 is sequence-independent and enhanced by DNA curvature. *EMBO J.* 31: 919–931.